On the Dynamics of the Leeuwin Current

ANDREW J. WEAVER AND JASON H. MIDDLETON

School of Mathematics, The University of New South Wales, Kensington, New South Wales, Australia

(Manuscript received 15 July 1988, in final form 30 November 1988)

ABSTRACT

Two models, one numerical and one analytical, are used to investigate mechanisms for the generation and flow of the Leeuwin Current observed off the west coast of Australia. Three numerical experiments are conducted using the Bryan-Cox Ocean General Circulation Model. In the first experiment an alongshore density gradient is imposed, while in the latter two experiments the additional effects of warm, fresh North West Shelf waters are considered. The alongshore density gradient in the Indian Ocean produces an onshore geostrophic flow which turns southward and intensifies as it flows along the coast of Western Australia and into the Great Australian Bight. Maximum alongshore surface velocities occur just off the shelf break and below this poleward current is a weak equatorward flow. The magnitudes of the velocity vectors and associated advection of temperature and salinity, and the width, structure and geographical location of the current all agree well with field observations. The effects of the warm, fresh North West Shelf waters are to enhance the alongshore barotropic current on the shelf. This response is mainly local and diminishes with alongshore distance. Model results suggest that the Leeuwin Current is a baroclinic current driven by an alongshore density gradient in the Indian Ocean, maintained by equatorward surface heating and poleward surface cooling. The numerical results further predict the existence of a cyclonic circulation off Northwest Cape in the top 120 m of water. It is deduced that the seasonal modification of the Leeuwin Current is due to local winds and seasonal variation in the north-south density gradient.

A linear analytical model of the continental shelf circulation coupled to a two layer open ocean confirms the conclusions drawn from the numerical model, and shows that the shelf circulation obeys a simple balance between alongshore pressure gradient forces (due to steric height gradients), and bottom friction. It is shown that in the absence of vertical mixing, the presence of a sloping shelf is necessary for the existence of the trapped eastern boundary current. Without the sloping shelf the current radiates offshore through baroclinic Rossby wave propagation. For parameters applicable to the Leeuwin Current, the analytic model predicts realistic alongshore transports.

1. Introduction

The Leeuwin Current (named by Cresswell and Golding 1980, after the *Leeuwin* which in 1662 was the first Batavia-bound Dutch ship to explore the Great Australian Bight) is a poleward flowing eastern boundary current which flows along the continental shelf edge off the west coast of Australia and into the Great Australian Bight (for an excellent review see Church et al. 1988). It is unlike other eastern boundary currents of the world oceans in that there is neither surface equatorward flow nor coastal upwelling (Wooster and Reid 1963). These other boundary currents (e.g., Peru, Benguela, California, Canary) are all part of a large-scale anticyclonic gyre that is driven by anticyclonic winds. Indeed Andrews (1977) noted the inertial nature of the Leeuwin Current over the continental shelf and drew analogies with western boundary currents.

There has been much experimental research conducted in the past that has led to a description of the important features of the Leeuwin Current. Satellite imagery studies (e.g., Legeckis and Cresswell 1981), drifter studies (e.g., Cresswell and Golding 1980) and water bottle and CTD studies (e.g., Rochford 1969a; Thompson and Cresswell 1983; Thompson 1984; Greig et al. 1986) indicate that warm, fresh water flows southward with maximum velocities near the shelf edge. Below the surface and off the shelf break there is an equatorward undercurrent. Offshore, the large-scale circulation of the Indian Ocean consists of an anticyclonic gyre (Thompson and Veronis 1983), although at 110°E between 15° and 30°S there is a persistent eastward inflow (Hamon 1965).

Several theories have been developed to explain the presence of the Leeuwin Current. Thompson and Veronis (1983) postulated that an alongshore wind on the northwest shelf could generate the Leeuwin Current. This hypothesis, however, was rejected by Thompson (1984), since in his experimental study, nowhere did he detect a poleward alongshore component of the wind. Thompson concluded that the Leeuwin Current is driven by alongshore steric height gradients at the shelf edge and later argued that bottom friction on the shelf was necessary for its existence

---

Corresponding author address: Dr. Andrew J. Weaver, Joint Institute for the Study of the Atmosphere and Ocean, University of Washington, AK-40, Seattle, Washington, 98195.

(Thompson 1987). Godfrey and Ridgway (1985) found observational evidence to support Thompson's theory. They suggested that Indonesian throughflow from the Pacific to the Indian Ocean may create the steric height gradient observed along the continental shelf. McCreary et al. (1986) rejected the possibility of remote forcing in the form of Indonesian throughflow since they argued that this would create a coastal current which would weaken away from the forcing region, a feature not observed with the Leeuwin Current. They went on to examine the possibility that thermohaline forcing due to a poleward increase of surface density in the ocean interior was the mechanism for the generation of the Leeuwin Current. Their model, an adaptation of McCreary (1981), led to a poleward surface current with an equatorward undercurrent of comparable magnitude to that which was observed. Kundu and McCreary (1986) examined in detail the idea of remote forcing of the Leeuwin Current by Indonesian throughflow. In particular, they forced their model with an inflow of 7.3 Sv (Sv ≡ 10^6 m^3 s^{-1}), which is of the order of the observed transport through the Indonesian archipelago. Without vertical mixing all the inflow continued across the ocean, and hence there was no eastern boundary current. When vertical mixing was included in the model, part of the inflow bent poleward generating a coastal circulation which diminished with alongshore distance. They concluded that Indonesian throughflow contributed to the Leeuwin Current but that it was not the dominant forcing mechanism.

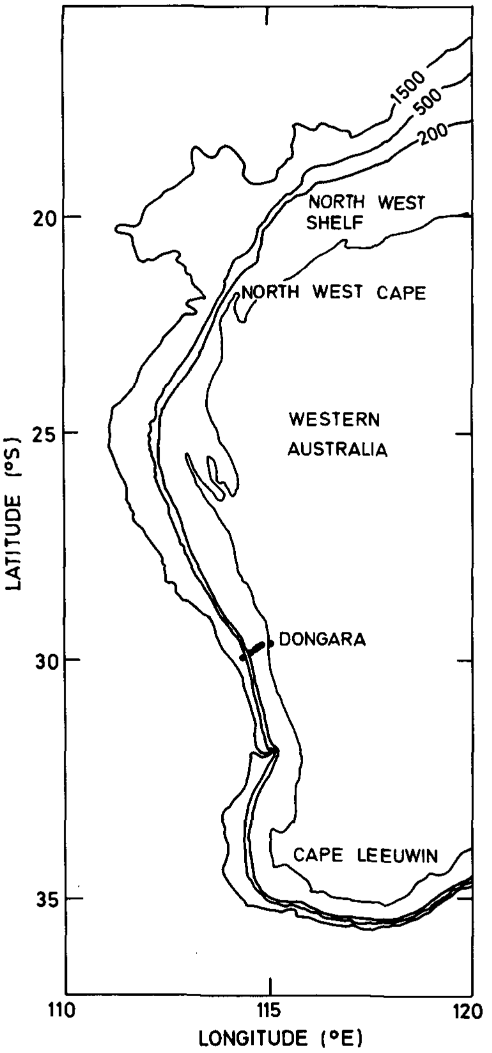

FIG. 1. Bathymetry off the coast of Western Australia showing the 200, 500 and 1500 m depth contours. The array of five current meter moorings used off Dongara during LUCIE is also shown.

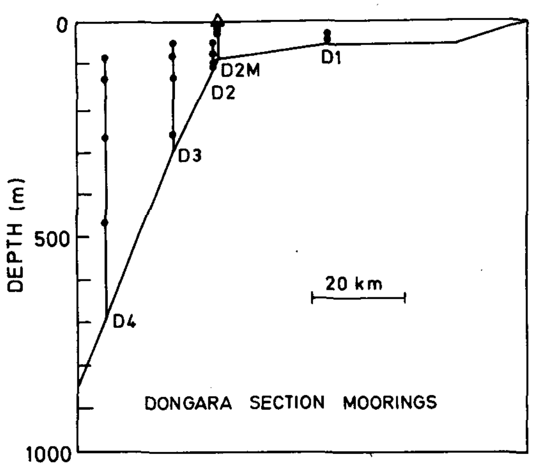

FIG. 2. Schematic diagram of the Dongara array at 29.5°S used in Period 1 of LUCIE. The depth of each current meter is given in Table 1 (the top current meter of D3 failed during Period 1). The array used during Period 2 was similar to Period 1 (Table 2) although the top current meter of D1 and the bottom current meter of D2M were lost. As in Period 1, the top current meter of D3 also malfunctioned. Redrawn from Boland et al. (1988).

The Leeuwin Current Interdisciplinary Experiment (LUCIE) was conducted between September 1986 and August 1987 (Church et al. 1988) in an attempt to provide a better description of the current and to understand the physical processes that govern its motion. Another major goal of LUCIE was to study possible influences of the current on the life cycles of marine species. As part of this experiment an offshore array of five current meter moorings was deployed off Dongara at 29.5°S (Fig. 1). This array proved especially useful since it provided a full year of current meter data. Boland et al. (1988) deployed the moorings for two 6-month periods. In the first period (September to February) the Leeuwin Current was weakest whereas in the second period (February to August) the Leeuwin Current was strongest. Figure 2, redrawn from Boland et al. (1988), shows the mooring deployment used at Dongara during LUCIE, and Tables 1 and 2 (also from Boland et al.) give the mean alongshore velocities at each meter over Period 1 and Period 2, respectively. It is apparent that in Period 1, when the southerly winds are maximum (Godfrey and Ridgway 1985; Holloway

TABLE 1. Alongshore component of velocity at the Dongara Array (29.5°S) used in LUCIE for Period 1 (September 1986 to February 1987). The data was taken from Boland et al. (1988). Refer to Figs. 1 and 2 for a description of the array. Negative values of v imply southward velocities. The top current meter of D3 failed during Period 1.

Mooring	Depth (m)	Mean v (cm s^{-1})	Length of record
D1	28	4.7	17 Sep–13 Jan
	43	2.1	17 Sep–30 Jan
D2M	8	3.3	17 Sep–2 Nov
	13	2.5	17 Sep–2 Nov
	23	−1.0	3 Oct–2 Nov
D2	48	−5.5	17 Sep–31 Jan
	73	−10.7	17 Sep–31 Jan
	93	−9.0	17 Sep–31 Jan
	103	−7.1	17 Sep–31 Jan
D3	75	−16.8	18 Sep–31 Jan
	125	−12.4	18 Sep–31 Jan
	250	2.3	18 Sep–31 Jan
D4	79	−6.4	18 Sep–31 Jan
	129	−1.9	18 Sep–31 Jan
	254	12.0	18 Sep–31 Jan
	454	14.5	18 Sep–31 Jan

and Nye 1985), the mean alongshore velocities are generally weaker than in Period 2. In fact, on the shelf at D1 the current is actually northward, but very weak. Average alongshore velocities of magnitude up to 38.5 cm s^{-1} are observed in Period 2 at D3. Despite the opposing winds, the Leeuwin Current accelerates as it flows poleward reaching mean alongshore speeds in excess of 50 cm s^{-1} near Cape Leeuwin (McCreary et al. 1986). In the deep water off the shelf (D4) the current is actually equatorward but weak, with maximum speed in Period 1.

The surface temperature structure of the Leeuwin Current, described above, is readily visible in satellite images. Figure 3 shows the sea surface temperature off Western Australia at 2340 (local time) on 15 June 1984, corresponding to Period 2. It is evident that warm North West Shelf waters are being advected along the western coast of Australia with maximum advection at the shelf break. These warm waters are further evident well into the Great Australian Bight. Strong temperature fronts can be seen at the seaward edge of the current and an eddy is present off Perth. Eddies can also be seen off the south coast.

In this paper we investigate numerically two possible theories for the generation of the Leeuwin Current. In the first experiment we consider the driving mechanism to be an alongshore density gradient, as observed in the Indian Ocean off Western Australia (Rochford 1969b; McCreary et al. 1986). In two other experiments we examine possible contributions from warmer, fresher waters from the North West Shelf, which are evident in the satellite image of Fig. 3. These warm, fresh North West Shelf waters are postulated to arise from Indonesian throughflow (Sharma 1972; Godfrey and Golding 1981; Godfrey and Ridgway 1985; Kundu and McCreary 1986). Church et al. (1988) discussed the seasonal nature of the throughflow from the Pacific to the Indian Oceans. Based on the work of Gentilli (1972) they argued that the throughflow in the Southern Hemisphere autumn and winter was isolated by a reversal of the flow in spring. They further argued that this water then achieved a thermal homogeneity over

TABLE 2. Alongshore component of velocity at the Dongara Array (29.5°S) used in LUCIE for Period 2 (February 1987 to August 1987). The data was taken from Boland et al. (1988). Refer to Figs. 1 and 2 for a description of the array. Negative values of v imply southward velocities. The top current meters of D1 and D3 and the bottom current meter of D2 failed during Period 2.

Mooring	Depth (m)	Mean v (cm s^{-1})	Length of Record
D1	43	−6.3	17 Feb–8 Aug
D2M	8	−17.0	9 Feb–10 Aug
	13	−16.2	9 Feb–10 Aug
D2	47	−19.3	17 Feb–8 Aug
	72	−17.9	17 Feb–8 Aug
	92	−17.9	17 Feb–8 Aug
	102	−8.1	17 Feb–8 Aug
D3	83	−38.5	17 Feb–8 Aug
	133	−29.8	17 Feb–8 Aug
	258	−0.9	17 Feb–8 Aug
D4	71	−30.3	17 Feb–9 Aug
	121	−24.3	17 Feb–9 Aug
	246	0.2	17 Feb–9 Aug
	446	5.9	17 Feb–9 Aug

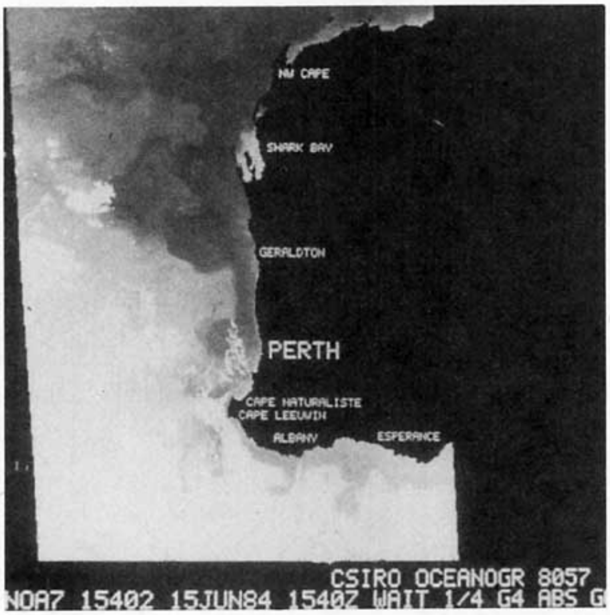

FIG. 3. Satellite image of the sea surface temperature off Western Australia. The image was taken at 2340 (local time) on June 15, 1984, corresponding to Period 2. Warmer waters are indicated by darker shades. There is some cloud present in the bottom left of the image. A tongue of warm water intrudes down the coast from the north and well into the Great Australian Bight. Notice also the presence of the warm North West Shelf waters.

the summer, becoming a *raft* of warm water, which spread southwards during the following autumn and winter. It is this raft of warm, less saline water that we model herein.

The results of the numerical model are strikingly similar to field observations. In particular, an eastward geostrophic flow (Hamon 1965) turns poleward near the shelf break to form a narrow current which in turn advects warm, fresh water from the north. There is also an equatorward undercurrent. The lighter North West Shelf waters enhance the barotropic current on the shelf. This response is mainly local and diminishes with alongshore distance. We are led to the conclusion that the Leeuwin Current is driven by an alongshore density gradient and is modified by the seasonal winds.

The outline of this paper is as follows: In section 2 we describe the numerical model and the three experiments. The results of the numerical experiments are presented in section 3 and compared to field observations and the data of Tables 1 and 2. In section 4 we introduce a linear analytical model of the continental shelf circulation coupled to a two layer open ocean and we examine the circulation arising from an imposed alongshore density gradient. A summary is presented in section 5.

2. Description of the numerical model

Three numerical experiments were conducted using the Cox (1984) version of the GFDL Bryan–Cox Ocean General Circulation Model (OGCM) with seven vertical levels. In the first experiment an initial north–south density gradient was imposed in the top 500 m of the entire model ocean. The ocean was then allowed to geostrophically adjust in the absence of external forcing. This geostrophic adjustment process therefore gives a good sense of the time development from an initial rest state. The geometry used in the first experiment is illustrated in Fig. 4a. The initial temperature and salinity data used in the model were interpolated from values given in Tables 3 and 4. These data were obtained from the annual mean data along 110°E of Rochford (1962, 1969b) and Levitus (1984).

In order to examine the possible influences of warm, relatively fresh North West Shelf waters on the circulation off the west coast of Australia, a second experiment was considered. In this experiment an imposed initial dam, separating warm, less saline North West Shelf waters from the surrounding Indian Ocean (dashed line in Figs. 4a, b), was removed instantaneously at time $t = 0$ (as in Weaver and Hsieh 1987). The fluid was then allowed to geostrophically adjust in the absence of external forcing. In this experiment the Indian Ocean water had the same initial T–S structure as in Experiment 1 (Tables 3 and 4). The assumed horizontally homogeneous raft of water was given the initial T–S structure of Table 5 (taken from northerly values of the Indian Ocean T–S data of Tables 3 and 4).

The topography used in the first two experiments assumed a somewhat idealized continental slope which was uniform in the alongshore direction (Fig. 4a). In

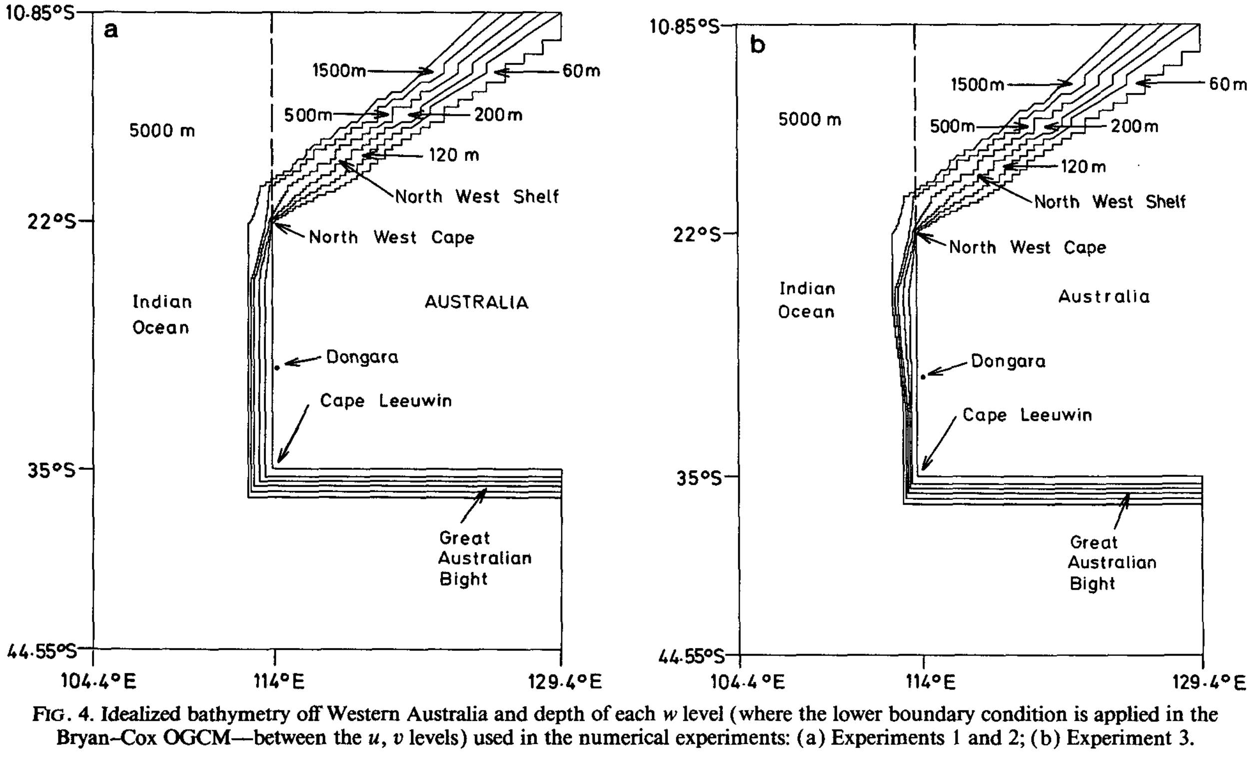

FIG. 4. Idealized bathymetry off Western Australia and depth of each w level (where the lower boundary condition is applied in the Bryan–Cox OGCM—between the u, v levels) used in the numerical experiments: (a) Experiments 1 and 2; (b) Experiment 3.

TABLE 3. Initial temperature (°C) data used in the three numerical runs described in the text. The temperature at the sixth level (1000 m) and the seventh level (3250 m) were everywhere initially set to 5.2° and 2.2°C.

Latitude (°S)	Depth				
	15 m	45 m	90 m	160 m	350 m
10	26.60	24.90	22.70	15.00	9.80
12	27.10	26.00	24.50	18.60	10.50
14	27.10	26.70	26.00	20.10	11.50
16	26.50	25.50	24.20	19.40	11.90
18	26.20	25.40	24.10	20.10	12.80
20	25.50	25.10	23.50	20.00	13.20
22	24.30	23.40	22.40	20.00	13.40
24	23.00	22.60	21.80	19.10	13.60
26	22.20	21.60	20.90	18.70	13.00
28	21.30	20.80	19.90	17.90	12.80
30	20.00	19.60	19.00	16.20	11.90
32	19.40	18.80	18.30	15.30	11.20
34	18.50	17.90	17.10	15.10	11.00
36	17.00	16.40	15.80	13.80	10.00
38	15.50	14.90	14.30	12.30	9.00
40	14.00	13.40	12.80	10.80	8.00
42	12.50	11.90	11.30	9.30	7.00
44	11.00	10.40	9.80	7.80	6.50
46	10.00	9.40	8.80	7.00	6.30

reality the coast narrows considerably as one progresses southward (Fig. 1). The third experiment therefore incorporates the narrowing shelf of Fig. 4b into Experiment 2.

In all three experiments variable grid spacing was employed, with the grid being 0.05° (offshore) by 0.1° (alongshore), all along the west coast of Australia from 22° to 35°S (Figs. 4a, b). The grid spacing was increased to a maximum of 0.4° by 0.75° at the northwest and southwest boundaries, and to 1.0° by 0.75° at the northeast and southeast boundaries. The boundary conditions employed by the Bryan–Cox OGCM at the solid boundaries are conventional, that is, no flow into or along boundaries (no-slip), and no flux of tracers (*T* and *S*) across boundaries. To eliminate high speed external gravity waves, the model uses the rigid-lid approximation. Bottom friction, which was assumed to be quadratic in velocity with a 10° turning angle (Gill 1982), was included in the model. Values for lateral eddy viscosity and diffusivity were set at 1.0×10^7 and $4.0 \times 10^6\ \mathrm{cm^2\ s^{-1}}$, respectively, while the vertical values were both set at $1\ \mathrm{cm^2\ s^{-1}}$. These values were used by Weaver and Hsieh (1987). In all three experiments the model was run with a 400 second timestep for an initial period of 40 days. The first and third experiments were run for an additional 40 days. The choices of grid spacing, eddy viscosity, timestep and level depths in the present model everywhere satisfy Killworth's topographic stability criterion (Killworth 1987). The kinetic energy density of the model began to level off at around 30 days in all three experiments (Fig. 5) and remained so for an additional 30 days in Experiments 1 and 3. By 80 days the transient features of the adjustment process appear to be decaying through the combined effects of viscosity and diffusion.

TABLE 4. Initial salinity (ppt) data used in the three numerical runs described in the text. The salinity at the sixth level (1000 m) and the seventh level (3250 m) were everywhere set initially to 34.70 ppt.

Latitude (°S)	Depth				
	15 m	45 m	90 m	160 m	350 m
10	34.22	34.30	34.56	34.60	34.70
12	34.25	34.35	34.45	34.62	34.65
14	34.36	34.40	34.55	34.68	34.82
16	34.55	34.65	34.80	34.92	35.00
18	34.70	34.80	34.95	35.02	35.15
20	34.94	34.96	35.03	35.19	35.28
22	35.10	35.15	35.30	35.50	35.33
24	35.25	35.30	35.48	35.62	35.35
26	35.50	35.56	35.65	35.78	35.35
28	35.60	35.63	35.70	35.75	35.25
30	35.70	35.75	35.83	35.70	35.15
32	35.78	35.81	35.70	35.53	35.05
34	35.60	35.70	35.60	35.40	34.95
36	35.42	35.60	35.60	35.30	34.90
38	35.25	35.45	35.50	35.20	34.85
40	35.10	35.16	35.21	35.10	34.80
42	34.95	35.00	35.05	35.00	34.75
44	34.86	34.86	34.90	34.80	34.70
46	34.65	34.65	34.66	34.68	34.70

TABLE 5. Initial temperature and salinity data used in Experiments 2 and 3 to model a warm, fresh pool of North West Shelf water possibly arising from Indonesian throughflow. This raft of water is to the east of the dashed line in Figs. 4a, b. The initial data for the lower two levels are the same as in the Indian Ocean region.

Depth (m)	Temperature (°C)	Salinity (ppt)
15	28.0	34.3
45	27.0	34.4
90	25.0	34.5
160	17.0	34.6
350	10.0	34.7

3. Results of the numerical experiments

Figures 6a–d and 7a–d illustrate the velocity fields at 10 day increments for Experiment 1 at the upper level (15 m) and the fifth level (350 m). As time progresses a western boundary current develops at the solid wall of the Indian Ocean (10° in longitude away from the region of interest) and an associated countercurrent is seen intensifying in time at the eastern edge of the western boundary current. This western boundary current is largely baroclinic and is driven by the initial alongshore density gradient although it has the same intensified structure as observed in the classic wind-driven model of Munk (1950). The largely baroclinic nature of the boundary current follows from the comparison with additional experiments (not shown here)

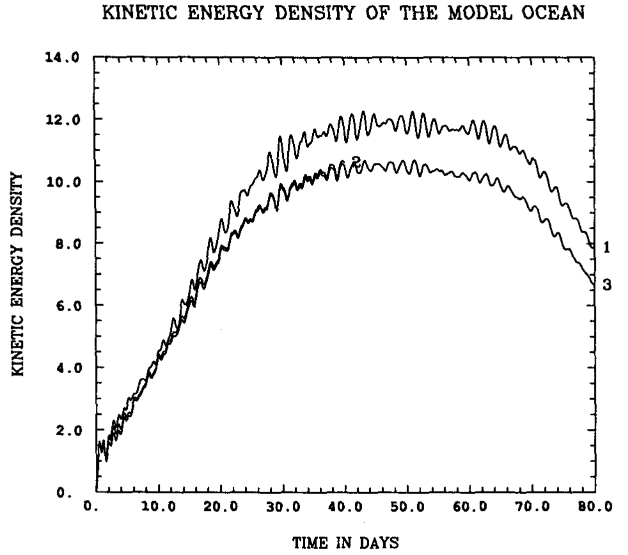

FIG. 5. Kinetic energy density (the total model kinetic energy divided by the total volume of the model basin) in 10^{-1} kg m^{-1} s^{-2} as a function of time. The numbers on the curves correspond to the experiment number. 1: Experiment 1, 2: Experiment 2 (as in Experiment 1 but with warm, fresh North West Shelf waters), 3: Experiment 3 (as in Experiment 2 but with a narrowing shelf).

in which the barotropic mode was removed at all times (i.e., there was no depth averaged flow). The structure of the western boundary current with depth is very similar for both the experiments with and without the barotropic mode. At the deepest level (3250 m—not presented) the current is weak and in the opposite direction. Eastward of the western boundary current and countercurrent the flow consists of an eastward geostrophically balanced flow at the upper level for all experiments at all time (Figs. 6a–d). This flow does not have uniform magnitude at all latitudes since the initial imposed density gradient is not constant (Tables 3 and 4). The western boundary current is a physically real feature of the present model (driven by an alongshore density gradient) but is of no further importance to the following discussion and analysis. In the initial adjustment process, however, Kelvin wave fronts are generated at the western boundary. These fronts propagate around the basin and form part of the transient response of the system. The evidence for the presence of the coastal Kelvin waves can be seen at the northern boundary of the model domain. At 10 days (Fig. 6a) the influence from these wave fronts appears to have propagated about half way along the northern boundary. By 20 days they appear to have reached the northeastern corner of the model (Fig. 6b), where they run into the continental shelf. On hitting the shelf these waves scatter into continental shelf wave modes and propagate southwestwards, reversing the shelf currents as they pass (Fig. 6c), all the while being damped by viscous effects. By 40 days their influence appears off the western coast of Australia as a substantial weakening of the southward flow. As we shall see later, the long term effect of this transient response is small.

For Experiment 1 we find that the eastward geostrophic flow in the Indian Ocean off Western Australia varies between 5 and 15 cm s^{-1}, as the initial north–south density gradient is not constant. On approaching the continental slope, this eastward current turns and forms a southward flowing boundary current which travels around the southwestern corner of Australia and into the Great Australian Bight (Fig. 6a). This boundary current intensifies with southward distance and at 10 days alongshore velocities of the order of 30 cm s^{-1} are observed. As time progresses (Fig. 6b) bottom friction retards the flow on the shelf, although near the shelf break the flow intensifies somewhat to around 35 cm s^{-1}. Furthermore, the eastward geostrophic flow weakens slightly in magnitude to between 4 and 8 cm s^{-1} as the adjustment process settles down. As time progresses still further (Figs. 6c, d), the boundary current substantially weakens with typical speeds of 24 cm s^{-1} at 30 days, and 17 cm s^{-1} at 40 days. This is primarily due to transient effects such as the coastal Kelvin waves initially generated at the western boundary.

At the fifth level (Figs. 7a–d) an equatorward current develops and intensifies with time as the deeper levels spin up. By 40 days (Fig. 7d) a well established northward flowing current extends all along the west coast of Australia. This equatorward undercurrent intensifies at 350 m with northward distance and reaches speeds of the order of 15 cm s^{-1}. It is interesting to note that at the sixth level (1000 m depth) the flow is also equatorward all along the western coast of Australia and is strongest at those latitudes of Figs. 7a–c where there is a transition from equatorward to poleward flow. This suggests that there is upwelling at 500 m into the fifth level because of the horizontal divergence, a feature confirmed by vertical velocity plots which are not presented here. The equatorward deep flow at 40 days is illustrated in Fig. 8 where maximum alongshore velocities of the order of 10 cm s^{-1} are observed at the southwestern shelf break.

Overall the magnitudes of the currents at ~20 days discussed above compare very favorably with the observations of Thompson (1984) and with the current meter data obtained in LUCIE (Tables 1 and 2). The general structure of the Leeuwin Current is portrayed, with a southward surface current deepening as it flows poleward, and a subsurface northward flow which rises as it flows equatorward (deduced from velocity plots at levels not included here). One very unsatisfactory problem is instantly apparent with the results of Experiment 1. This is the inability of the Leeuwin Current to maintain itself in intensity for a long period of time (Fig. 6d). There are several possibilities that exist for overcoming this problem. The first is that the duration of the numerical experiments is too short to adequately

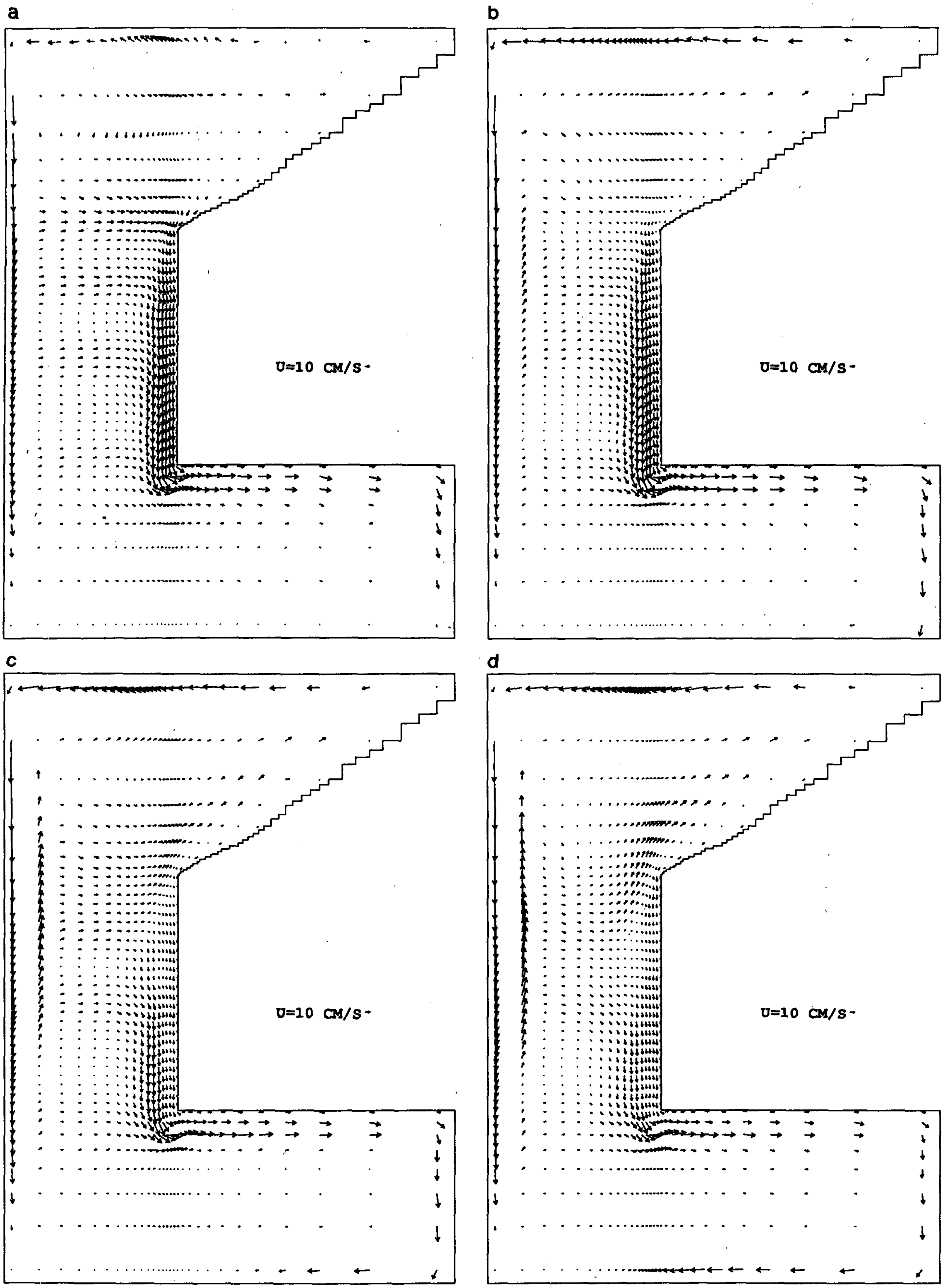

FIG. 6. Velocity vectors at the upper level (depth 15 m) for Experiment 1 at time (a) $t = 10$ days, (b) $t = 20$ days, (c) $t = 30$ days, (d) $t = 40$ days. In all the velocity fields that are presented (Figs. 6–11 and 14–15) velocity vectors are plotted at every fourth grid point in x and every fifth grid point in y to avoid clutter.

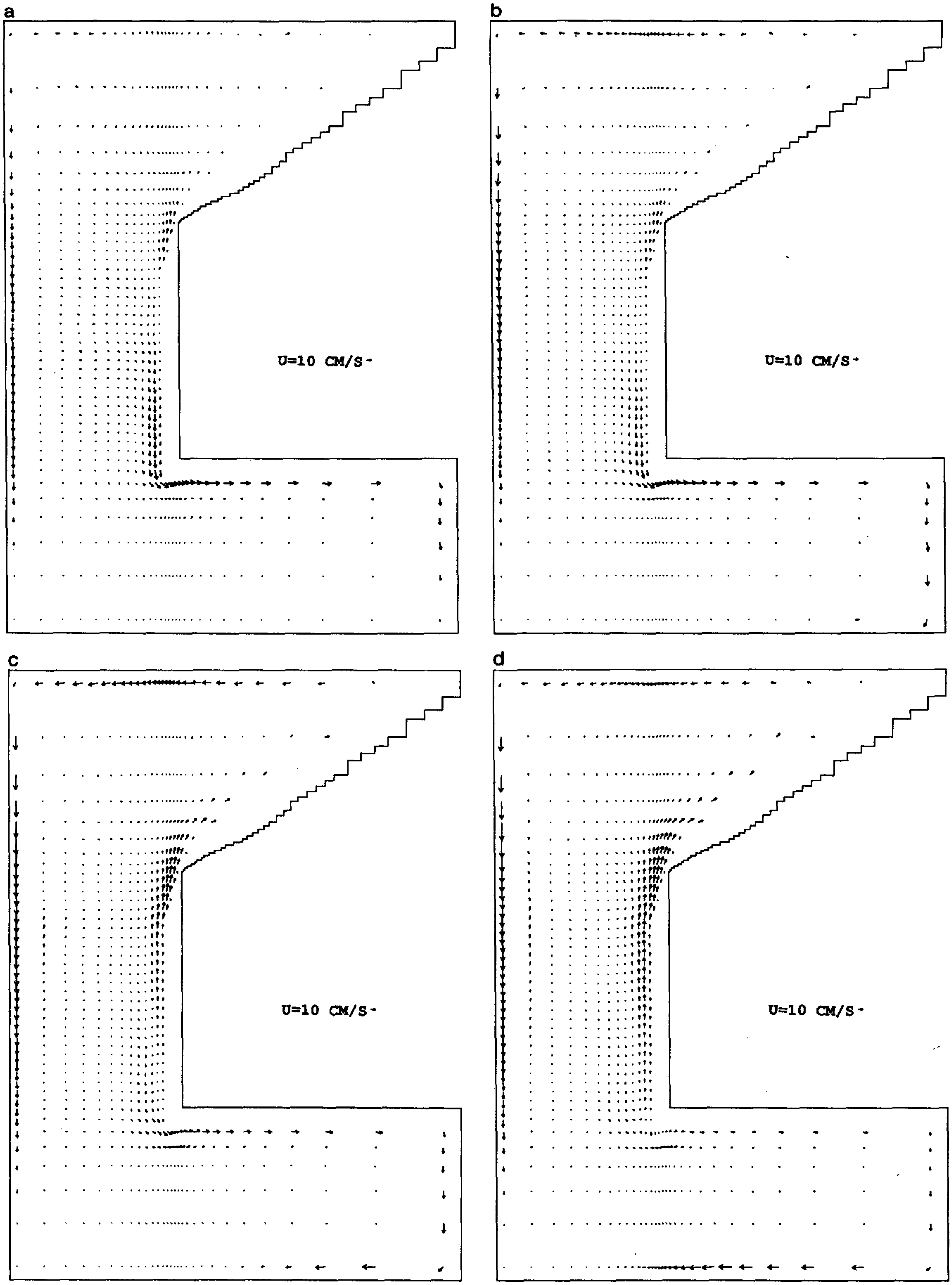

FIG. 7. As in Fig. 6 but at the fifth level (depth 350 m).

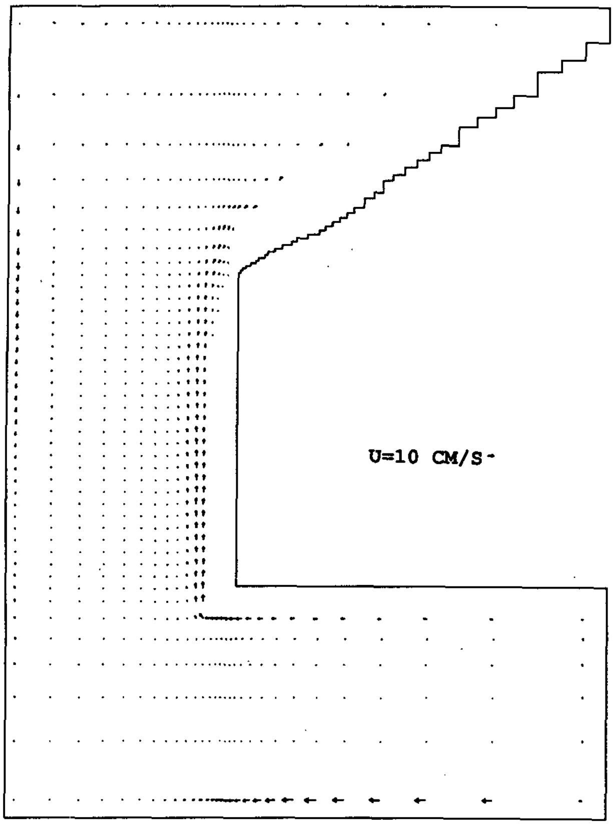

FIG. 8. Velocity vectors at the sixth level (depth 1000 m) for Experiment 1 at t = 40 days.

resolve the dynamics of the Leeuwin Current. At 40 days the solution appears to still be largely dominated by transient processes. Later in this section we will extend the numerical integrations for another 40 days to examine this problem. The second possibility, which we will now investigate, is that warm, fresh waters from the North West Shelf (possibly arising from Indonesian throughflow) provide a remote source for driving the Leeuwin Current. A third (which we will not investigate here) is direct forcing through surface heating/cooling.

Figures 9a and 9b illustrate the 30-day velocity fields at the upper level for Experiments 2 and 3. When warm, fresh North West Shelf waters are added (Figs. 4a, b; Table 5) to Experiment 1 the eastern boundary current is initially very similar in structure. At 30 days (Fig. 9a, cf., Fig. 6c) the boundary current is still intense, with maximum southward velocities of 23 cm s^{-1} at the northern edge of the coast and 29 cm s^{-1} at the southern edge. The influence of the warm, fresh raft of water can be seen to enhance the barotropic flow on the shelf (deduced from level 2 and 3 velocity plots not shown) in the neighborhood of North West Cape. This phenomenon tends to dominate over the transient response of the Kelvin waves discussed earlier. A strong cyclonic circulation can also be seen just off the North West Cape where the onshore geostrophic flow encounters the initial front. When the shelf is narrowed the boundary current moves nearer to the coast and continues to flow with maximum velocities near the shelf break (Fig. 9b, cf. Fig. 9a). Otherwise, the flow field appears largely unaffected by the shelf width. Once more the predicted current speeds in Experiments 2 and 3 are very similar to those observed by Thompson (1984) and in LUCIE (Tables 1, 2), however, the general structure is somewhat more accurate than that obtained in Experiment 1 at similar times.

At deeper levels a return equatorward flow is also observed in the two additional experiments (Figs. 10a, b for Experiments 2 and 3 at 30 days). For all the experiments the flow at the sixth level (depth 1000 m) is everywhere equatorward at the shelf break (not shown). Maximum northward velocities occur in the regions of weak northward velocities seen in Figs. 10a, b. Once more this implies that, as the subsurface current flows northward, it upwells between levels 5 and 6 as a result of the horizontal divergence at the level above. Similarly, as the surface current flows southward it deepens and intensifies. In comparing Fig. 10a to Fig. 7c, we see that the presence of the warm, fresh North West Shelf waters has little effect on the deep subsurface flow, as is to be expected, and the effect of the narrow shelf is simply to steer the subsurface flow (Fig. 10b, cf. Figs. 7c, 10a). In both Experiments 2 and 3, velocities at deep levels are similar to those observed in Experiment 1.

Figures 11a and 11b illustrate the velocity field at the upper level and fifth level, respectively, for Experiment 3 at 40 days. In comparing the surface flow at 40 days (Fig. 11a) with the surface flow at 30 days (Fig. 9b), we see that the warm, fresh water has further enhanced the barotropic flow on the shelf, with typical southward velocities of the order of 30 cm s^{-1} off North West Cape. Again this effect is most pronounced in the region of the forcing. The strong cyclonic circulation off the North West Cape has also been enhanced. Off the shelf the current appears to be weakening (now around 25 cm s^{-1} off Cape Leeuwin) and to be spreading westward. In fact, near Cape Leeuwin the 40 day velocity field is quite similar for both Experiment 1 (Fig. 6d) and Experiment 3. At the fifth level the velocity field is the same as for Experiment 1 (Fig. 7d), except that now the subsurface equatorward current is steered by the narrowing shelf.

As mentioned in the Introduction one of the most important characteristics of the Leeuwin Current is that it advects warm, fresh water along the coast of Australia and into the Great Australian Bight. Figures 12a–d illustrate temperature contours (in °C) at 10 day intervals for the top level of Experiment 1 (similar features occur at deeper levels). At 10 days (Fig. 12a) contours have been advected around 200 km southward at the eastern boundary. At 20 days (Fig. 12b) contours have been advected around 500 km southward at the southern tip of Western Australia where the current is stron-

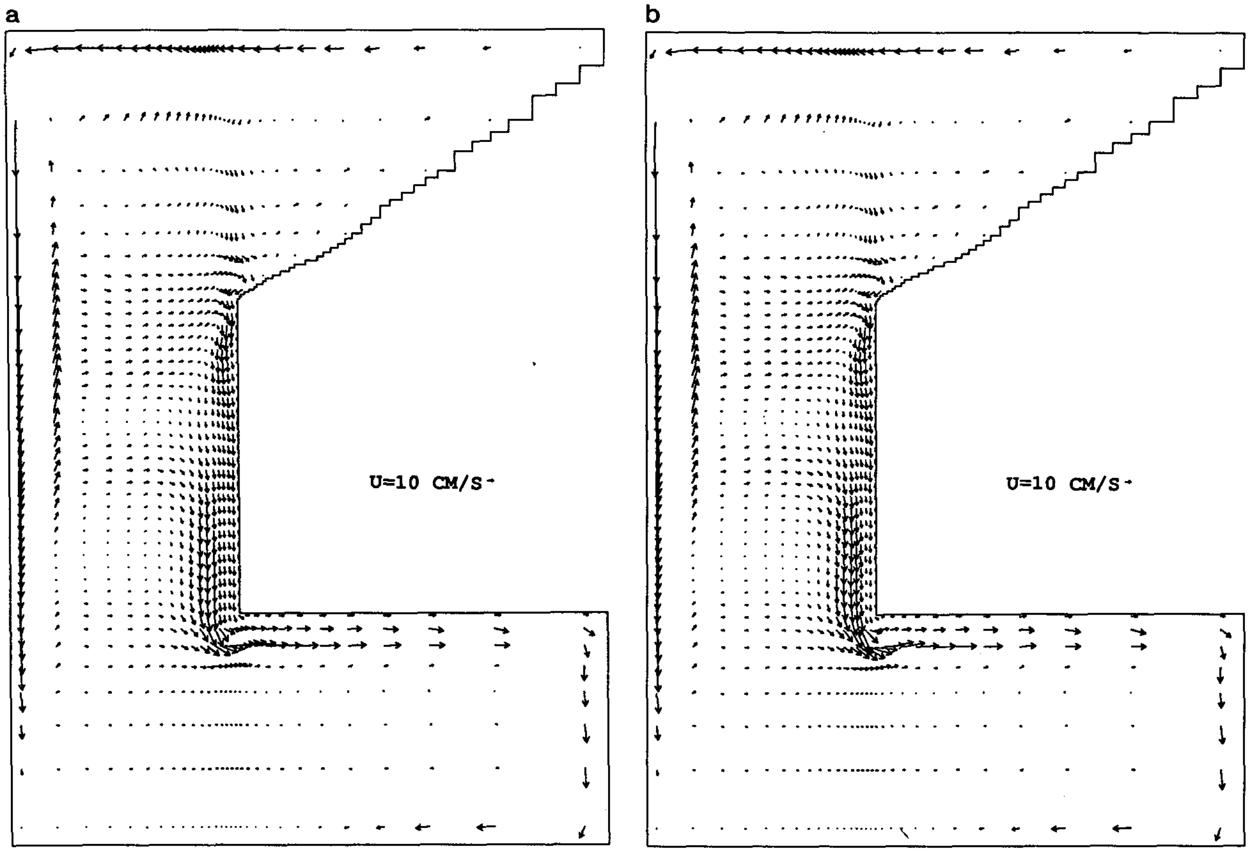

FIG. 9. Velocity vectors at the upper level (depth 15 m) at t = 30 days for (a) Experiment 2 (as in Experiment 1 but with warm, fresh North West Shelf waters); (b) Experiment 3 (as in Experiment 2 but with a narrowing shelf).

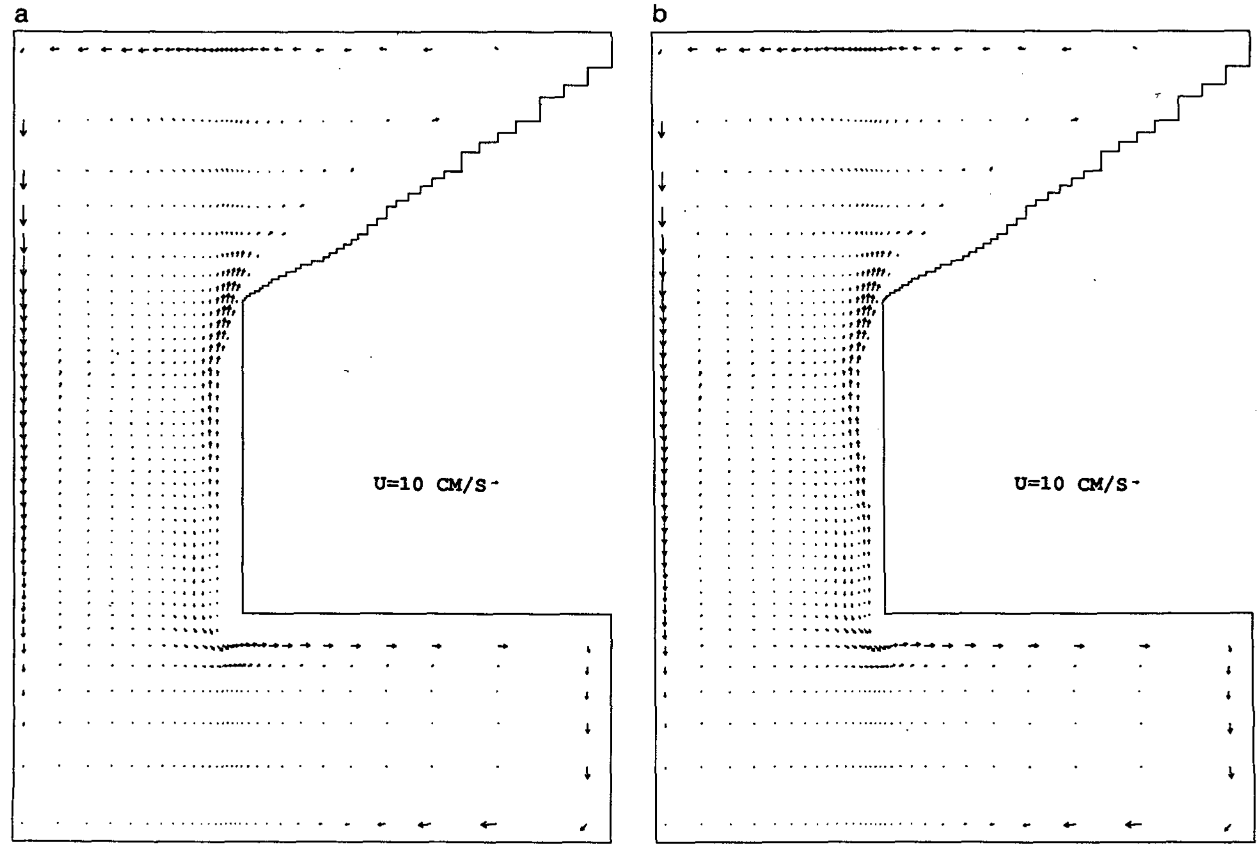

FIG. 10. As in Fig. 9 but at the fifth level (depth 350 m).

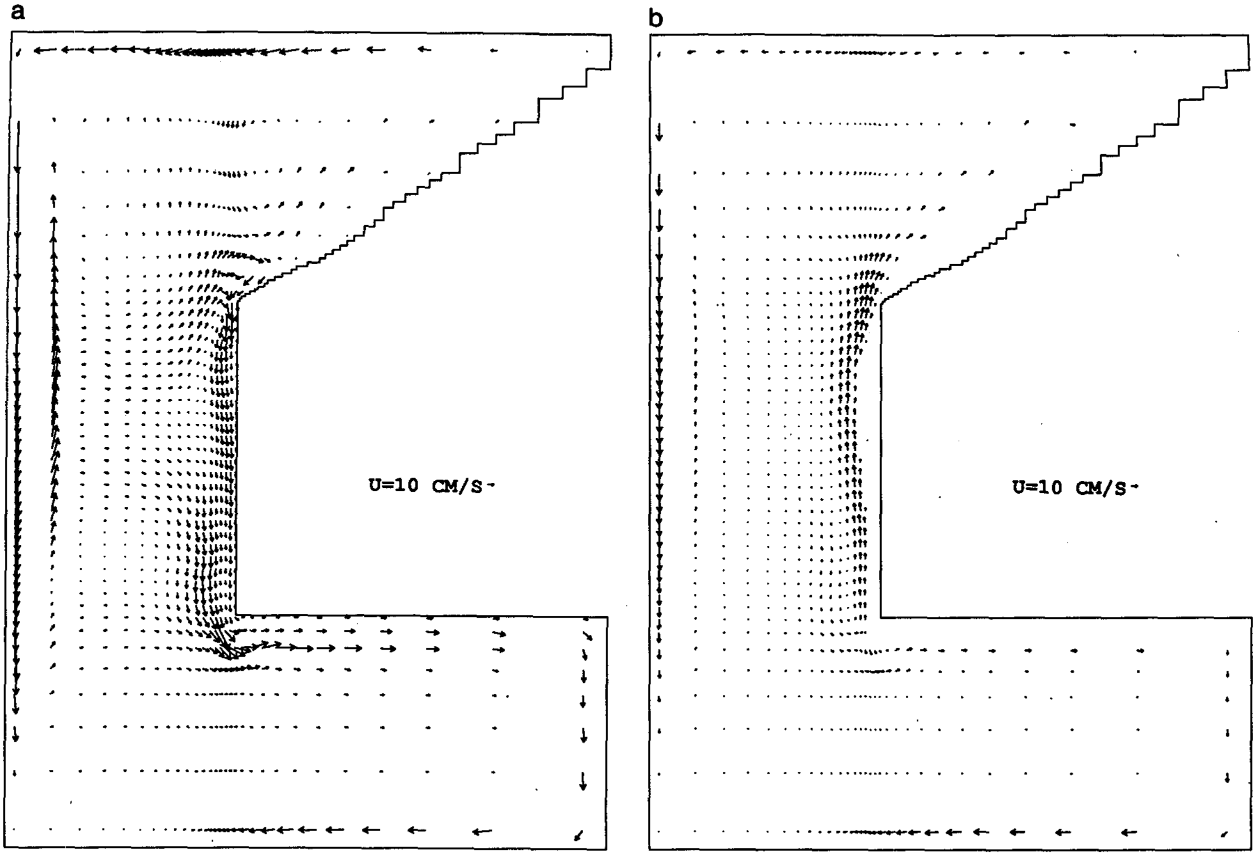

FIG. 11. Velocity vectors for Experiment 3 (as in Experiment 1 but with a narrowing shelf and warm, fresh North West Shelf waters) at $t = 40$ days: (a) upper level (depth 15 m); (b) fifth level (depth 350 m).

gest (Fig. 6c). This warm water is clearly seen to flow into the Great Australian Bight. At longer times (Figs. 12c, d) the advection process continues although it slows down considerably as the eastern boundary current weakens. Very strong temperature fronts (of the order of 2° across the front) occur at the western edge of the boundary current. The advection of warm water associated with the western boundary current and countercurrent is also apparent in Figs. 12a–d. When we include warm, fresh North West Shelf waters and a narrowing shelf into the problem (Experiment 3) a strong temperature front occurs at the northwestern tip of Australia, and this propagates southward with time (Fig. 13, cf. Fig. 12c). Maximum advection now occurs closer to the coast since the shelf is narrower.

The same features described above were observed in salinity plots which have not been included. Fronts with across-front salinity differences of around 0.5 ppt at the northwestern tip and 0.3 ppt at the southwestern tip of Australia occur at the western edge of the boundary current. Fresh, northern waters are initially advected very swiftly in Experiment 1, although the advection process weakens as the alongshore current weakens. The effects of the narrowing shelf and North West Shelf waters are exactly as described above for temperature.

The results from the numerical integrations so far still do not capture fully the dynamics of the Leeuwin Current. It appears that transient responses in the adjustment process are still important after 40 days. Even when we include remote forcing in the form of a raft of warm, fresh water, the resulting flow field is not entirely satisfactory. The initially generated strong coastal circulation appears to be leaking offshore slowly through baroclinic Rossby wave propagation. Even though vertical mixing is included in the numerical model, thereby damping the baroclinic Rossby modes in the direction of their group velocity, the current appears to slowly broaden westward (Fig. 11a, cf. Fig. 9b and Fig. 6d, cf. Fig. 6c). McCreary et al. (1986) and Kundu and McCreary (1986) discuss in detail the importance of vertical mixing in the trapping of their model eastern boundary currents. McCreary et al. (1986) further point out an alternative method for trapping the eastern boundary current, namely by forcing with annual frequency wind and surface density fields, thereby eliminating Rossby waves poleward of the critical latitude. As we shall see in the analysis of the next section, steady state trapped coastal currents driven by an alongshore density gradient (with no vertical mixing) exist in the presence of a sloping shelf (and are realistic if bottom friction is included), only

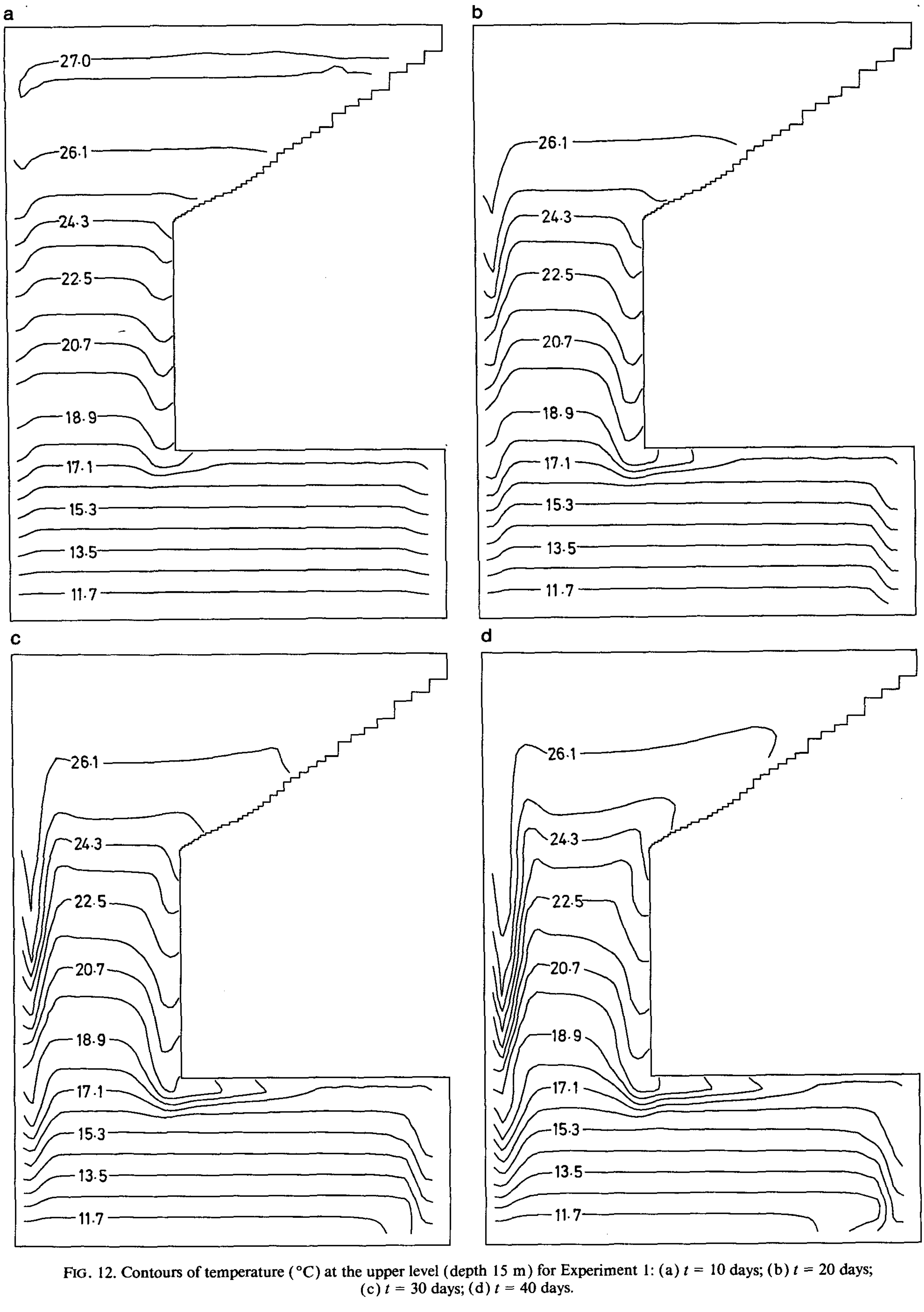

FIG. 12. Contours of temperature (°C) at the upper level (depth 15 m) for Experiment 1: (a) t = 10 days; (b) t = 20 days; (c) t = 30 days; (d) t = 40 days.

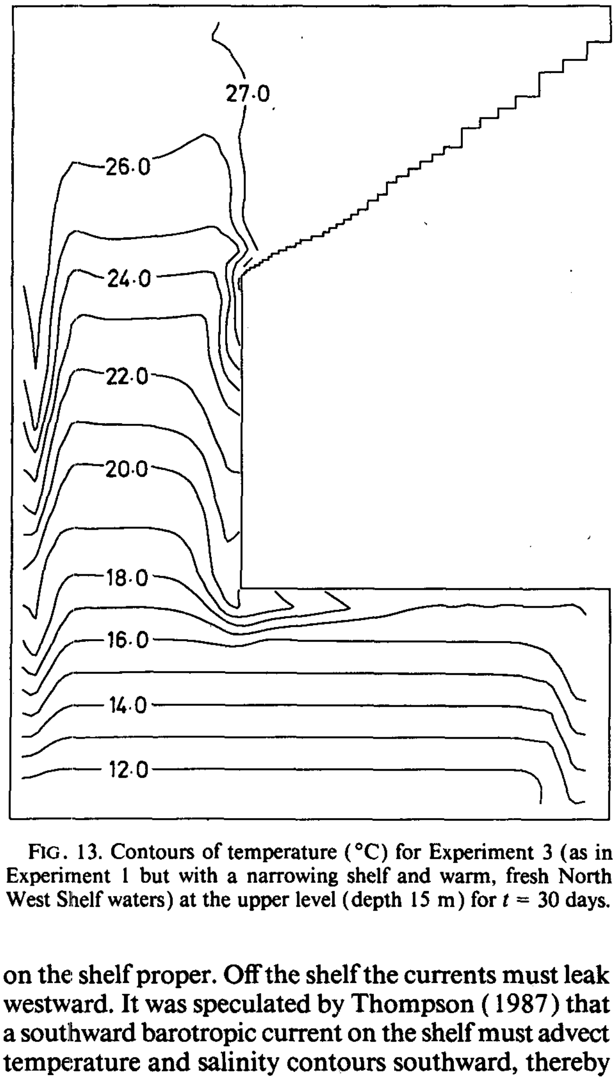

FIG. 13. Contours of temperature (°C) for Experiment 3 (as in Experiment 1 but with a narrowing shelf and warm, fresh North West Shelf waters) at the upper level (depth 15 m) for $t = 30$ days.

on the shelf proper. Off the shelf the currents must leak westward. It was speculated by Thompson (1987) that a southward barotropic current on the shelf must advect temperature and salinity contours southward, thereby generating thermal winds which would significantly enhance the poleward surface flow seaward of the barotropic maximum. Bearing this in mind we should expect the results of our numerical integration to look very similar to the Leeuwin Current since bottom friction, a sloping shelf, and vertical mixing are all incorporated into the model. For this reason we carried out integrations for another 40 days for both Experiments 1 and 3 (the results for Experiment 2 can be deduced from those of Experiments 1 and 3), in the hope that transient processes will have decayed away. The kinetic energy density graph of Fig. 5 gives us confidence that this is indeed the case, with the total energy in the model basin decaying through frictional effects even though (as we shall see later) the Leeuwin Current is intensifying.

Figures 14a and 14b illustrate the surface velocity field for Experiments 1 and 3 at 80 days, while Figs. 15a and 15b are for the corresponding experiment at the fifth level. For Experiment 1 (Fig. 14a) a strong southward flowing boundary current is well established off Western Australia, intensifying and deepening as it flows poleward. Maximum alongshore velocities of the order of 20 cm s^{-1} off North West Cape increase to order 40 cm s^{-1} off Cape Leeuwin, with peak velocities at the shelf break. As the current flows around Cape Leeuwin it meanders (cf. Fig. 3). The current at 80 days for Experiment 3 (Fig. 14b) is very similar to that for Experiment 1. The influence of the warm, fresh raft of water can readily be seen to enhance the barotropic flow in the vicinity of the North West Cape. This effect diminishes with alongshore distance. As the current flows and deepens southwards, it moves closer to the coast, due to the narrowing shelf, meanders, and intensifies. Alongshore velocities around 28 cm s^{-1} off North West Cape intensify to over 50 cm s^{-1} off Cape Leeuwin. At deeper levels the equatorward undercurrent has become well established. For both Experiment 1 (Fig. 15a) and Experiment 3 (Fig. 15b) the structure is quite similar. As this undercurrent flows northwards it hugs the shelf break, rises and weakens somewhat. Typical velocities are between 5 and 10 cm s^{-1} all along the western coast of Australia.

The agreement between the numerical results presented at 80 days and the field observations is excellent. The magnitudes of both the surface and subsurface components of the Leeuwin Current compare very favorably with the mean velocity observations discussed earlier. In both Experiments 1 and 3, a further feature that occurs is the development of a strong cyclonic circulation at the upper levels off North West Cape.

To complete the discussion of the numerical results we should compare the vertical structure of the model, predicted at 29.5°S, to the mean data observed in Period 2 of LUCIE (Table 2). Figure 16 shows contours of the alongshore component of velocity off Dongara, indicating the location of the surface maximum at the shelf break, the weaker alongshore flow on the shelf, and the deep subsurface equatorward flow. The vertical structure of the Leeuwin Current at 29.5°S, as predicted by the numerical model, is illustrated in the contours of the north–south velocity at 30, 40 and 80 days in Figs. 17a, b, c for Experiment 1 and in Figs. 18a, b, c for Experiment 3. For Experiment 1 (Fig. 17a), the initially strong poleward flow is observed trapped at the shelf break and a strong barotropic flow is seen on the shelf proper (cf. Fig. 6c). At deeper levels the equatorward flow can be seen hugging the shelf break. As time progresses further (Fig. 17b) the offshore flow broadens and drifts westward through baroclinic Rossby wave propagation, while on the shelf, the poleward barotropic flow intensifies somewhat. Deeper down the equatorward flow has intensified. After an additional 40 days (Fig. 17c), by which time transient processes have decayed, the surface flow has once more intensified at the shelf break while the deeper equatorward flow has weakened slightly. Since the alongshore barotropic flow on the shelf remains large during the transient stages of the model spinup, temperature and

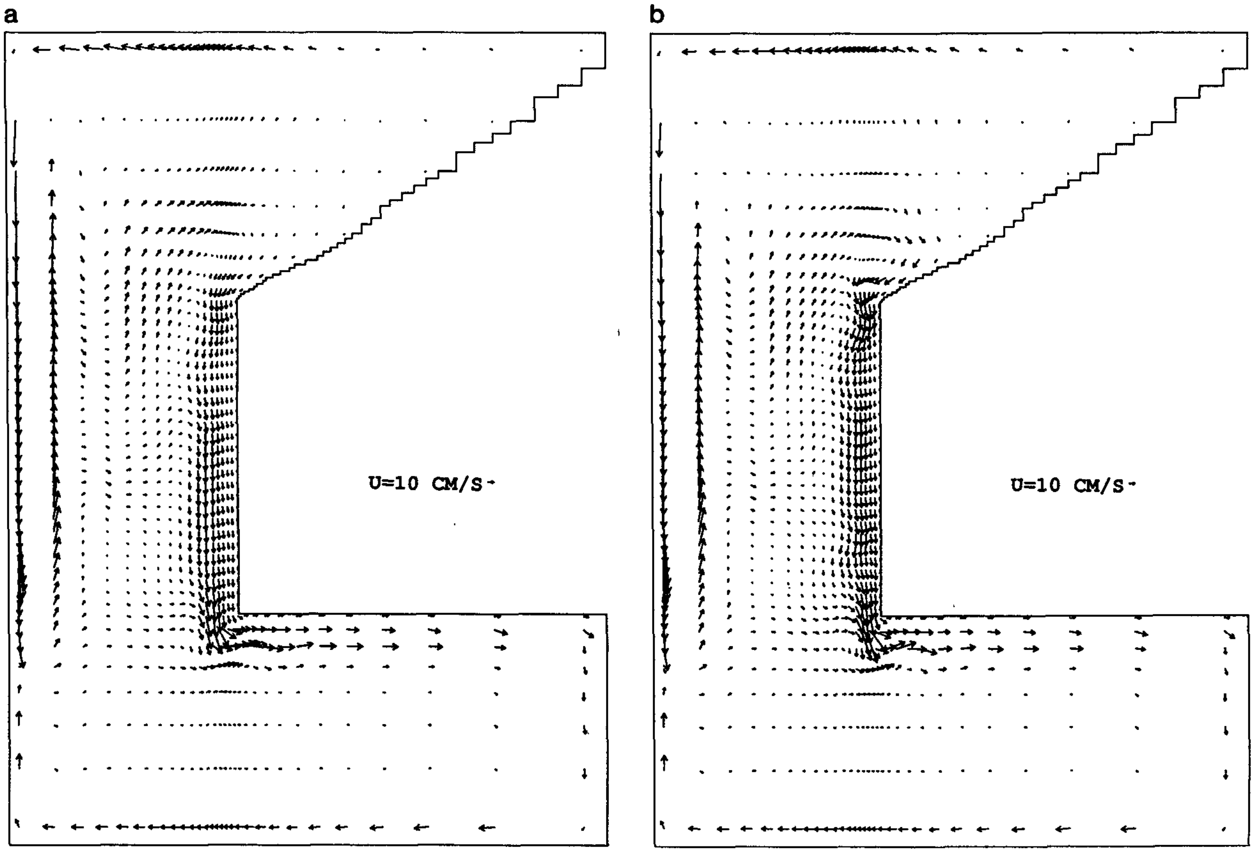

FIG. 14. Velocity vectors at the upper level (depth 15 m) at t = 80 days: (a) Experiment 1; (b) Experiment 3.

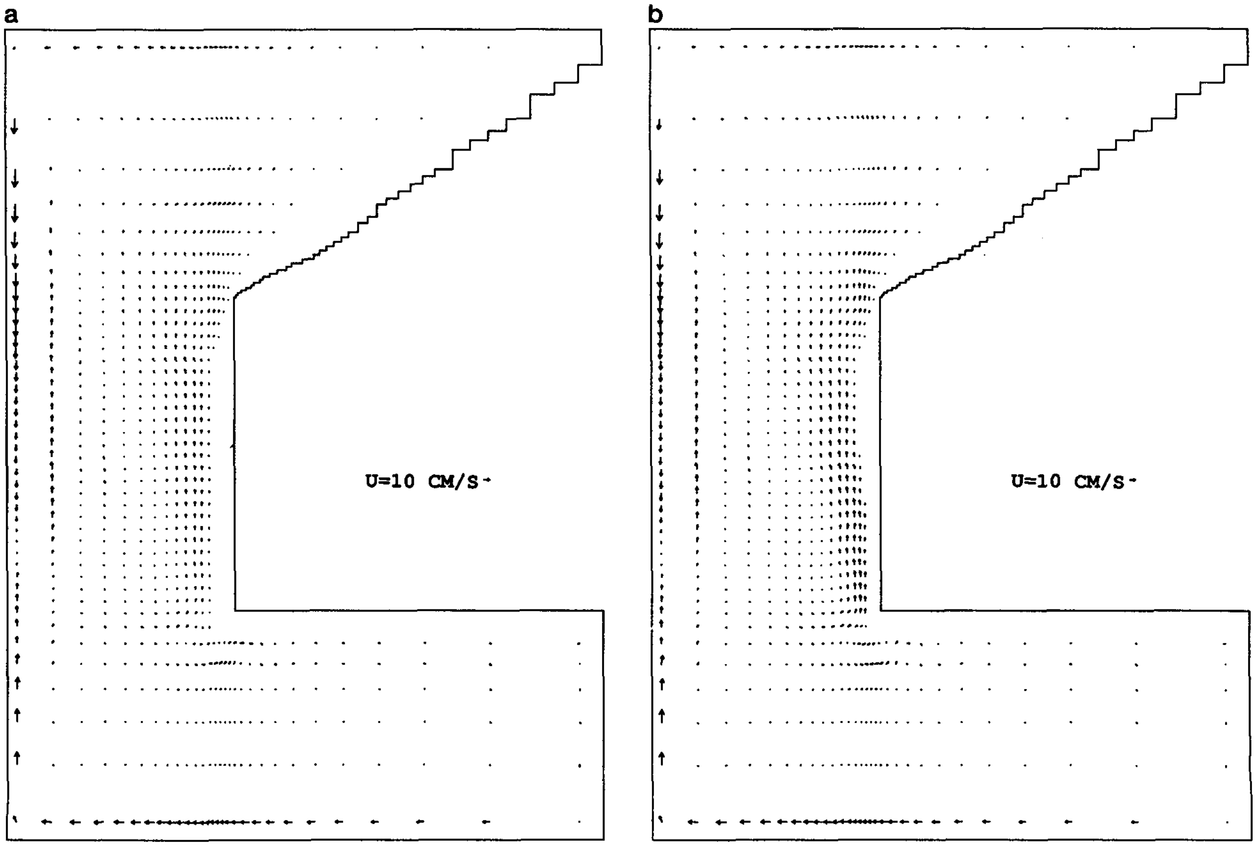

FIG. 15. Velocity vectors at the fifth level (depth 350 m) at t = 80 days: (a) Experiment 1; (b) Experiment 3.

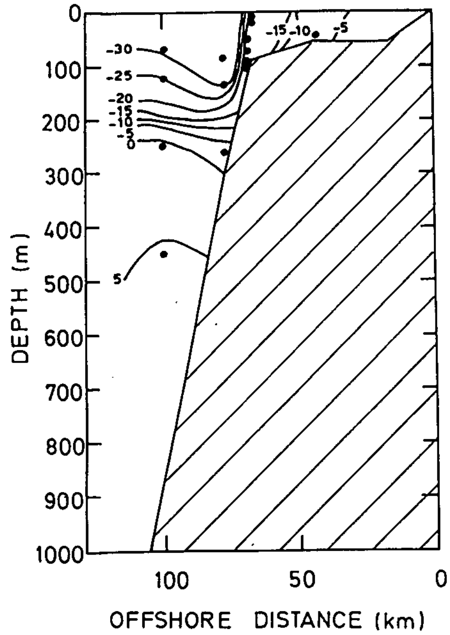

FIG. 16. Contours of the alongshore component of velocity from the section off Dongara (29.5°S) used in LUCIE. The contours are in cm s^{-1} with negative values corresponding to southward velocity. The data are taken for Period 2 (February 1987 to August 1987) from Table 2. The dots indicate the current meters (see Fig. 2 and Table 2) that were deployed by Boland et al. (1988).

salinity contours are still being advected southward, thereby creating strong offshore thermal/saline gradients. These gradients therefore generate thermal winds that significantly enhance the poleward flow seaward of barotropic shelf velocity maximum. This argument was originally proposed by Thompson (1987) and is clearly verified in movies that were made showing the vertical structure of the north–south component of the model velocities off Dongara (as shown in Figs. 17 and 18), with frames at half-day intervals.

For Experiment 3 the same features are observed. At 30 days (Fig. 18a), a shelf trapped flow is observed which broadens and propagates westward with time (Fig. 18b). All the while the barotropic flow on the shelf is intensifying, advecting temperature and salinity contours southward and thereby enhancing the poleward flow seaward of the current maximum. By 80 days (Fig. 18c) a velocity field similar to that of Experiment 1 (Fig. 17c) is set up. Now the current maximum is trapped nearer to the shore as the shelf has narrowed. Since the shelf is narrowing in Figs. 18a–c there is an eastward component of velocity (e.g., Fig. 14b), so that the alongshore magnitudes of the predicted Leeuwin Current are slightly larger than those portrayed in these figures.

The structure of the predicted (Figs. 17c and 18c) and observed (Fig. 16) Leeuwin Current are remarkably similar. In both cases there is a strong southward flow trapped at the shelf break. At depths greater than about 350 m there is an equatorward undercurrent and at the shelf break there is strong horizontal shear in the current.

In the next section we show how many of the features of the Leeuwin Current discussed in the present section can be reproduced using a simple linear model. In particular, the numerical results presented in this section at 80 days appear to look very much like a slightly modified, nonlinear version of the linear solutions of the next section.

4. Circulation driven by an alongshore density gradient

In this section we examine analytically the steady state circulation on a continental shelf driven by an unchanging alongshore density gradient. Our analysis is based upon that of Csanady (1985) and Vennell and Malanotte-Rizzoli (1987). In this paper, however, we introduce a finite width shelf and couple this region to a two layer ocean as in the wind driven model of Godfrey (1984).

a. The solution on the continental shelf

We start with the equations for steady low Rossby number flow on a continental slope governed by the equations (Csanady 1985),

$$-fv = -g\frac{\partial\zeta}{\partial x} - g\int_z^0 \frac{\partial\epsilon}{\partial x}dz + \frac{1}{\rho_0}\frac{\partial\tau_x}{\partial z}, \qquad (1)$$

$$fu = -g\frac{\partial\zeta}{\partial y} - g\int_z^0 \frac{\partial\epsilon}{\partial y}dz + \frac{1}{\rho_0}\frac{\partial\tau_y}{\partial z}, \qquad (2)$$

where the coordinates x, y and z are oriented in the offshore, alongshore and vertical directions, respectively (Fig. 19). Here u and v are the horizontal velocity components in the x and y directions, ζ is the sea level displacement, f is the Coriolis parameter and g is the acceleration due to gravity. The components of the Reynolds shear stress in the horizontal plane are given by (τ_x, τ_y). The parameter ρ_0 is a reference density and $\epsilon = (\rho_1 - \rho_0)/\rho_0$ is the proportionate density excess, where ρ_1 is the density of the fluid. We now use the long-wave approximation in which the cross-shelf length scale is assumed small compared to the alongshore length scale, so that we may neglect cross-shelf bottom stress. Furthermore, we assume that there are no surface wind stresses. If we depth integrate (1) and (2) assuming further that the density anomaly ϵ is independent of depth we obtain

$$-fV = -g\zeta_x h - \frac{g}{2}\epsilon_x h^2, \qquad (3)$$

$$fU = -g\zeta_y h - \frac{g}{2}\epsilon_y h^2 - \frac{1}{\rho_0}\tau_{yb}, \qquad (4)$$

where U and V are the depth integrated or transport components of the horizontal velocities and h is the

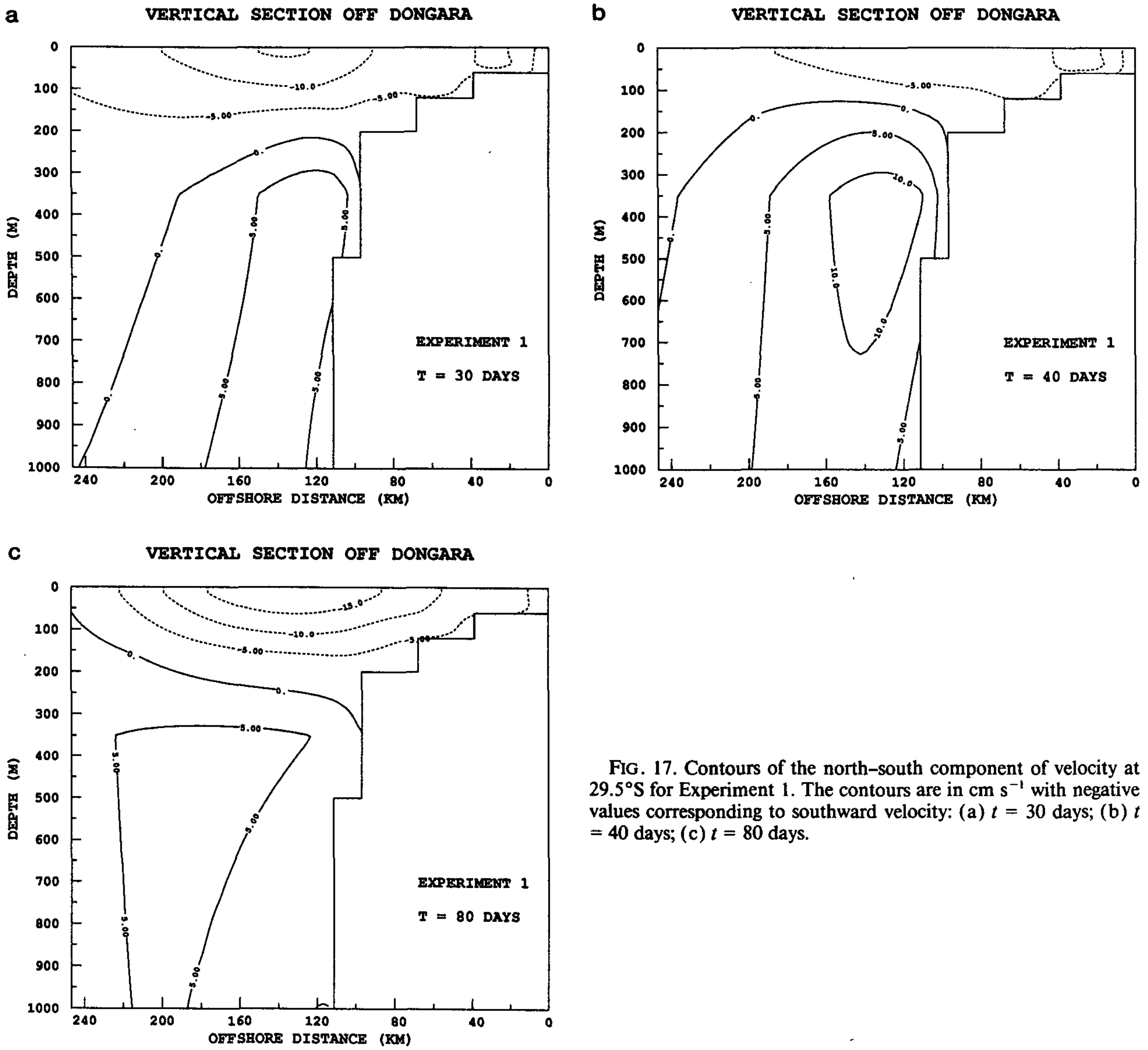

FIG. 17. Contours of the north–south component of velocity at 29.5°S for Experiment 1. The contours are in cm s^{-1} with negative values corresponding to southward velocity: (a) t = 30 days; (b) t = 40 days; (c) t = 80 days.

depth of the fluid. Following Csanady (1979, 1985) we parameterize the bottom shear stress by

$$\frac{\tau_{yb}}{\rho_0} = \frac{rg}{f}\left(\frac{\partial \zeta}{\partial x} + \int_{-h}^{0} \frac{\partial \epsilon}{\partial x}\,dz\right), \tag{5}$$

where r is a bottom friction coefficient. Since ϵ is independent of depth, equation (5) reduces to

$$\frac{\tau_{yb}}{\rho_0} = \frac{rg}{f}(\zeta_x + \epsilon_x h). \tag{6}$$

Thus we may write (3) and (4) as

$$fV = g\zeta_x h + \frac{g}{2}\epsilon_x h^2, \tag{7}$$

$$fU = -g\zeta_y h - \frac{g}{2}\epsilon_y h^2 - \frac{rg}{f}(\zeta_x + \epsilon_x h). \tag{8}$$

We now choose a linear bottom depth profile which is uniform in the alongshore direction, so that $h = h(x) = sx$. Furthermore, we wish to consider coastal circulation driven by an alongshore density anomaly. Thus, we take $\epsilon = \alpha y$ with α constant. We choose $x = 0$ to be the coast and $x = l$ to be the shelf break (Fig. 19). The northern extent of the model region is taken as $y = 0$, so that the density anomaly increases as we move southward (positive y). Under the above assumptions (7) and (8) become

$$fV = gsx\zeta_x, \tag{9}$$

$$fU = -gsx\zeta_y - \frac{gs^2\alpha}{2}x^2 - \frac{rg}{f}\zeta_x. \tag{10}$$

Furthermore, continuity implies

$$U_x + V_y = 0. \tag{11}$$

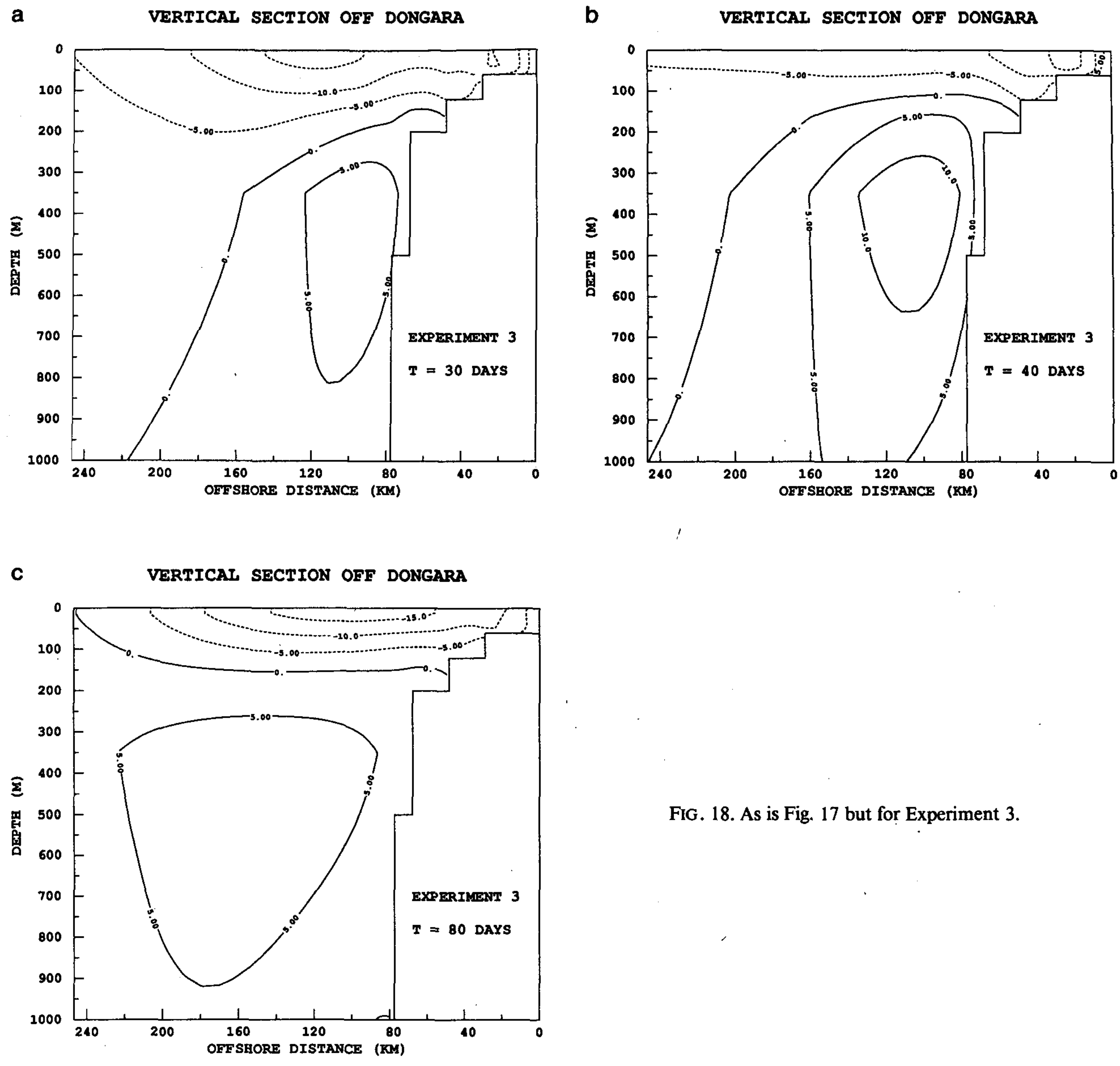

FIG. 18. As is Fig. 17 but for Experiment 3.

Equations (9)–(11) are nearly identical to those used by Vennell and Malanotte-Rizzoli (1987).

To obtain a single equation in ζ we cross-differentiate (9) and (10), assuming we are on an f-plane (Southern Hemisphere, $f < 0$), and substitute the result into (11). This procedure gives

$$\zeta_{xx} - \gamma\zeta_y - \delta x = 0, \qquad (12)$$

where

$$\gamma = \frac{|f|s}{r}, \quad \delta = \frac{\alpha|f|s^2}{r}. \qquad (13)$$

Middleton and Thomson (1985) studied the effects on steady continental shelf circulation of allowing the Coriolis parameter f to vary with alongshore distance y. In particular, they generalized Csanady's arrested topographic wave model (Csanady 1978) to include the β-effect. Their analysis showed that on an eastern boundary in the Southern Hemisphere the β-effect simply reduced the trapping of the boundary current, i.e., it became broader than in the f-plane case (considered herein). We conclude therefore that on the shelf β will be of little dynamical importance. This of course is not true in the open ocean model of section 4b.

The boundary condition for (12) at $x = 0$ follows from (10) since at $x = 0$ there can be no transport into or out of the coast. This boundary condition is then

$$\zeta_x = 0 \quad \text{at} \quad x = 0. \qquad (14)$$

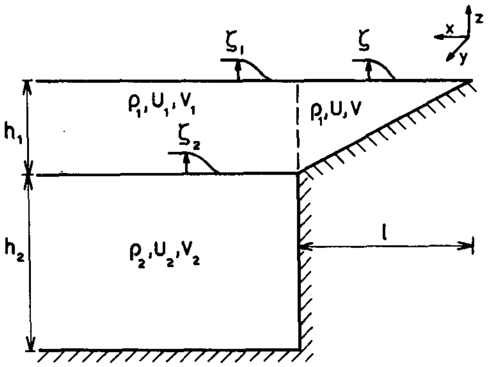

FIG. 19. Schematic diagram of the linear model used to examine the circulation driven by an alongshore density gradient.

At the northern extreme of the region ($y = 0$) we specify that there is no transport into the model domain ($V = 0$ at $y = 0$). Since (12) can be transformed into a homogeneous heat equation (interpreting time as y), the above restriction states that the circulation in our model domain ($0 \leqslant x \leqslant l$, $0 \leqslant y < \infty$) is not affected by the circulation for $y < 0$. From (9) this boundary condition may be written as

$$\zeta_x = 0 \quad \text{at} \quad y = 0. \tag{15}$$

The final boundary condition which we use is at the shelf break ($x = l$). In section 4b we will match the shelf solution to a two layer open ocean in which there is also an imposed density anomaly. Since at $x = l$ we must have continuity of U and ζ, the last term on the right of (10) must vanish (cf. 28). Thus

$$\zeta_x = 0 \quad \text{at} \quad x = l. \tag{16}$$

Here we have assumed that the undisturbed upper layer depth in the open ocean, h_1 (Fig. 19), is given by $h_1 = sl$. If $h_1 > sl$ then (16) would also involve ζ_y and the problem would be mathematically more complicated.

Equation (12) may be transformed by making the substitution

$$\zeta = \eta + \frac{\delta}{6}x^3 \tag{17}$$

to obtain the homogeneous heat equation

$$\eta_{xx} - \gamma\eta_y = 0 \tag{18}$$

with boundary conditions

$$\eta_x = 0 \quad \text{at} \quad x = 0, \tag{19}$$

$$\eta_x = -\frac{\delta}{2}l^2 \quad \text{at} \quad x = l \tag{20}$$

and *initial condition*

$$\eta_x = -\frac{\delta}{2}x^2 \quad \text{at} \quad y = 0. \tag{21}$$

Since both the boundary conditions at $x = 0$ and $x = l$ and the initial condition at $y = 0$ are written in terms of η_x, we seek a solution in the form of a Fourier cosine series,

$$\eta(x, y) = \sum_{n=1}^{\infty} a_n e^{-(c_n{}^2/\gamma)y} \cos c_n x + A_0 + B_0 y + C_0 x^2. \tag{22}$$

The coefficients a_n, eigenvalues c_n and constants B_0, C_0 are determined by substituting (22) into (18)–(20) and expanding the right side of (21) into a Fourier sine series. This procedure gives

$$\eta = -\frac{\delta l}{2\gamma}y - \frac{\delta l}{4}x^2 - \frac{2\delta l^3}{\pi^4}\sum_{n=1}^{\infty}\frac{(1 - \cos n\pi)}{n^4} \times e^{-(n^2\pi^2/\gamma l^2)y}\cos\frac{n\pi}{l}x + A_0, \tag{23}$$

where A_0 is an arbitrary constant. We must include the arbitrary constant A_0 since (18) is a heat equation, so that the solution propagates forward in *time* (positive y). Given a knowledge of η at $y = 0$, we determine η for all $y > 0$. Our initial condition (21) only specifies a condition on η_x. Without loss of generality we choose $A_0 = 0$. The transformation (17) and the two equations (9) and (10) thus give

$$\zeta = -\frac{\delta l}{2\gamma}y - \frac{\delta l}{4}x^2 + \frac{\delta}{6}x^3 - \frac{2\delta l^3}{\pi^4}\sum_{n=1}^{\infty}\frac{(1 - \cos n\pi)}{n^4} \times e^{-(n^2\pi^2/\gamma l^2)y}\cos\frac{n\pi}{l}x, \tag{24}$$

$$U = -\frac{2gs\delta l}{\gamma f\pi^2}\left\{x\sum_{n=1}^{\infty}\frac{(1 - \cos n\pi)}{n^2} \times e^{-(n^2\pi^2/\gamma l^2)y}\cos\frac{n\pi}{l}x - \frac{l}{\pi} \times \sum_{n=1}^{\infty}\frac{(1 - \cos n\pi)}{n^3}e^{-(n^2\pi^2/\gamma l^2)y}\sin\frac{n\pi}{l}x\right\}, \tag{25}$$

$$V = \frac{gs\delta}{2f}x\left\{x^2 - lx + \frac{4l^2}{\pi^3}\sum_{n=1}^{\infty}\frac{(1 - \cos n\pi)}{n^3} \times e^{-(n^2\pi^2/\gamma l^2)y}\sin\frac{n\pi}{l}x\right\}. \tag{26}$$

b. The solution in the open ocean

We model the open ocean as a two-layer fluid, which consists of an upper layer of density ρ_1 and undisturbed depth h_1, overlying a motionless ($U_2 = V_2 = 0$), deep ($h_2 \gg h_1$) lower layer of density ρ_2 (Fig. 19). Then the governing reduced gravity transport equations are

$$\frac{\partial U_1}{\partial t} - fV_1 = -gh_1\frac{\partial \zeta_1}{\partial x}, \tag{27}$$

$$\frac{\partial V_1}{\partial t} + fU_1 = -gh_1 \frac{\partial \zeta_1}{\partial y} - \frac{gh_1{}^2}{2}\epsilon_y, \qquad (28)$$

$$g'\left(\frac{\partial U_1}{\partial x} + \frac{\partial V_1}{\partial y}\right) = -g\frac{\partial \zeta_1}{\partial t}, \qquad (29)$$

where U_1 and V_1 are the transports in the offshore (x) and alongshore (y) directions, respectively. Here ζ_1 is the sea level displacement,

$$g' = \frac{(\rho_2 - \rho_1)}{\rho_2} g$$

is the reduced gravity and $f = f_0 - \beta y$ is the Coriolis parameter (Fig. 19). The interfacial displacement is given by

$$\zeta_2 = \frac{(g' - g)}{g'} \zeta_1$$

and as in the last section, the imposed density anomaly gradient is taken to be $\epsilon_y = \alpha$. Since the internal deformation radius is small compared to the scale of variation of the density anomaly and as we consider seasonal time scales that are long compared to the time for a large-scale internal Rossby wave to travel one deformation radius, we may neglect the time dependent terms of (27) and (28).

To obtain a single equation in ζ_1 we cross-differentiate (27) and (28) and substitute the result into (29) using (27). This procedure gives

$$\frac{\partial \zeta_1}{\partial t} + C\frac{\partial \zeta_1}{\partial x} = 0, \qquad (30)$$

where

$$C = \frac{g'\beta h_1}{f^2} \qquad (31)$$

is the phase speed of an internal Rossby wave. The solution to (30) is therefore

$$\zeta_1(x, y, t) = \zeta_1\left(l, y, t - \frac{x - l}{C}\right), \qquad (32)$$

which gives the open ocean response to sea level variations at the shelf break.

Suppose we now assume that the density anomaly on the shelf is held constant for a sufficiently long period of time. The solution (32) then gives

$$\zeta_1(x, y) = \zeta_1(l, y). \qquad (33)$$

c. *The complete solution*

Let us define

$$\zeta_0 = \zeta, \quad U_0 = U \quad \text{at} \quad x = l \qquad (34)$$

where ζ and U in (34) are the shelf slope solutions (24) and (25), respectively. The boundary conditions which must be satisfied are continuity of offshore/onshore transport and sea level displacement. Thus

$$U_1 = U_0, \quad \zeta_1 = \zeta_0 \quad \text{at} \quad x = l. \qquad (35)$$

Since ζ_1 is independent of x, it follows that U_1 is independent of x and so

$$\zeta_1 = \zeta_0, \quad U_1 = U_0, \quad V_1 = 0 \quad \text{for} \quad x > l. \qquad (36)$$

We have thus calculated the full solution. For $0 \leqslant x \leqslant l$ (continental shelf) the solution is given by (24)–(26), whereas for $x > l$ (open ocean) the solution is given by (36), where ζ_0 and U_0 are defined by (34).

We choose parameters that typify the west coast of Australia. Specifically, we choose l = 110 km and h_1 = 200 m so that $s = 1.818 \times 10^{-3}$. The Coriolis parameter is taken at 28°S to be $f = -6.847 \times 10^{-5}$ s^{-1} and the acceleration due to gravity is taken to be 9.8 m s^{-2}. The reduced gravity is assigned $g' = g \times 10^{-3}$ and the frictional coefficient r is taken to be $r = 4 \times 10^{-4}$ m s^{-1} (both from Godfrey 1984). The imposed density gradient is calculated from the observed annual mean temperature and salinity data of Rochford (1962, 1969b). We assume that the temperature drops from 27.10° to 16.0°C and the salinity increases from 34.10 to 35.78 ppt over 1445 km, so that $\alpha = 2.94 \times 10^{-9}$ m^{-1}.

Figure 20a portrays contours of ζ and ζ_1 in 10^{-3} m and Figs. 20b and 20c give contours of U, U_1 and V, respectively, in m^2 s^{-1}. In all three of these plots the vertical dashed line represents the shelf break and the vertical solid line represents the coast.

In the far field Eq. (26) gives

$$V = \frac{gs\delta}{2f} x\{x^2 - lx\}. \qquad (37)$$

For the parameters given above this has a maximum amplitude of $V = 43$ m^2 s^{-1} at $x = \frac{2}{3}l$ and corresponds to a depth averaged velocity of 32 cm s^{-1} there. Equation (37) is inversely proportional to the friction coefficient r. If we choose $r = 2 \times 10^{-4}$ m s^{-1}, as in Csanady (1985), then $V = 86$ m^2 s^{-1} at $x = \frac{2}{3}l$ and the depth averaged velocity is equal to 64 cm s^{-1}.

It is evident in comparing Figs. 20b, c to the numerical results for large time discussed earlier (Figs. 14a, b), that the main features of the continental shelf circulation are well described by the present linear model. In particular there is a weak geostrophically balanced onshore flow which turns and flows south. This southward flow intensifies with alongshore distance and peaks near the shelf break. The depth averaged velocities of around 32 cm s^{-1} are comparable to the magnitudes observed in both the earlier numerical experiments and in field observations (Thompson 1984, Table 2). Furthermore, the sea level drop over 1445 km (the length of the western coast of Australia) is about 50 cm (as observed by Godfrey and Ridgway

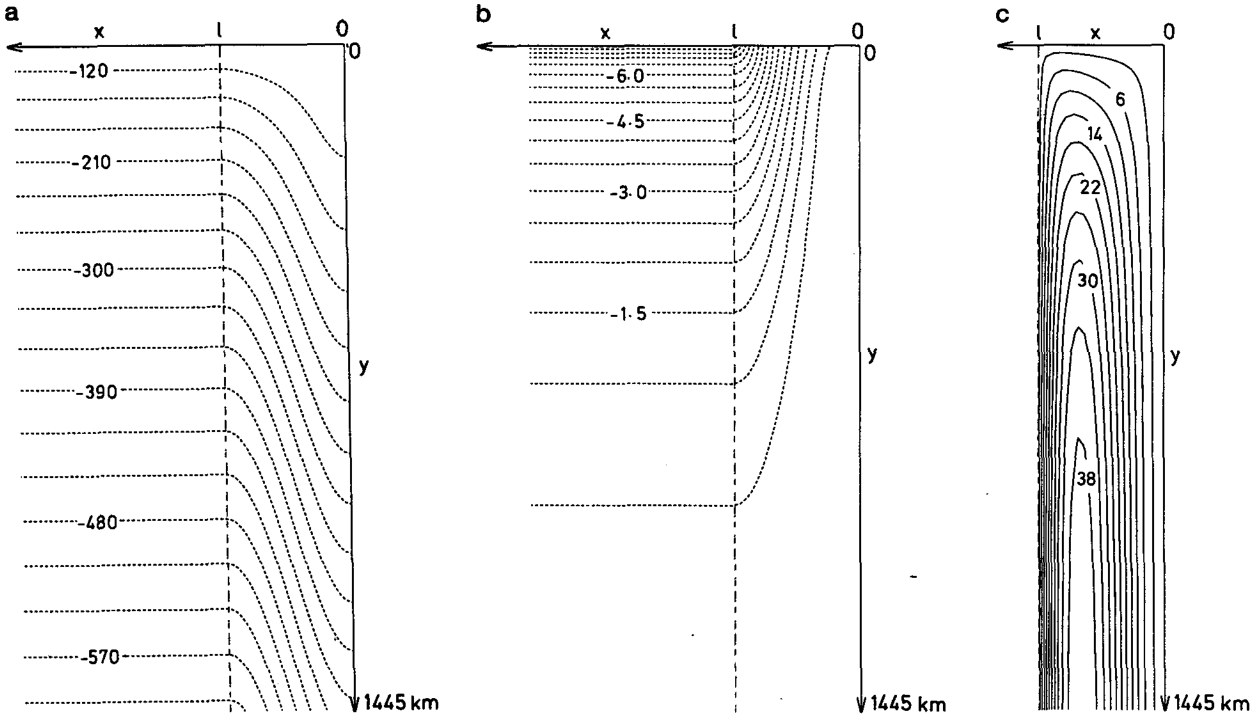

FIG. 20. Contours of the solutions to the linear problem for the parameters of section 4: (a) Sea level elevation (in 10^{-3} m); (b) zonal transport U (in $m^2 s^{-1}$); (c) alongshore transport V (in $m^2 s^{-1}$). The dashed line represents the shelf break and the solid line represents the coast. Positive y corresponds to the southward direction (see Fig. 19).

1985; McCreary et al. 1986). In considering Fig. 20a it should be noted that we must interpret all sea level elevations relative to the value at $y = 0$ due to the analogy between (18) and the heat equation. Unfortunately, the linear model of this section is unable to predict the weak subsurface equatorward flow. This is a result of the boundary condition at $x = l$ and the nature of our matching to the open ocean.

In interpreting the physics of our analytical model let us consider two limiting cases pointed out by an anonymous referee and Stuart Godfrey. Suppose first that there was no continental shelf, so that the ocean boundary was a vertical wall. Then the solution (36) applies everywhere with $U_0 = 0$. It is straightforward to show from (28) that in this case

$$U_1 = 0, \quad V_1 = 0, \; \zeta_1 = -\frac{h_1}{2}\epsilon, \tag{38}$$

where we have arbitrarily set the constant in integrating (28) to zero. Thus the surface layer adjusts (through transient westward baroclinic Rossby wave propagation) to balance the imposed density anomaly and there is no current. This is consistent with the models of McCreary et al. (1986) and Kundu and McCreary (1986) in the limit of no vertical mixing. Thus the sloping shelf must be important to the dynamics.

Now consider the case on the shelf when there is no bottom friction ($r = 0$) so that (12) and (14)–(16) simplify to

$$\zeta_y + \alpha s x = 0, \tag{39}$$

$$\zeta_x = 0 \quad \text{at} \quad y = 0 \tag{40}$$

i.e., the boundary conditions at $x = 0$ and $x = l$ are irrelevant. The solution to (39) and (40) and the associated transports U and V can easily be shown to be

$$\zeta = -\alpha sxy, \quad U = -\frac{g\alpha s^2 x^2}{2|f|}, \; V = \frac{g\alpha s^2 xy}{|f|}. \tag{41}$$

Only in the case $h_1 = sl$ can we match this to our two-layer open ocean model. In this case (36) is once more valid and hence

$$\zeta_1 = -\alpha sly, \quad U_1 = -\frac{g\alpha s^2 l^2}{2|f|}, \; V_1 = 0. \tag{42}$$

In the case of no bottom friction, a nonzero coastal circulation still exists. Maximum alongshore velocities now occur at the shelf break and the alongshore transport V increases linearly with alongshore distance, as it is fed by a meridionally uniform onshore geostrophic transport U_1. In our original solution (with bottom friction), the net onshore transport vanishes as y gets large (Fig. 20b). This follows since the onshore flow in the top half of the upper layer is eventually identically balanced by an offshore Ekman transport in the lower half of the upper layer. Nevertheless, the fact that we have obtained trapped solutions with zero bottom friction shows that the presence of the sloping shelf is necessary for the alongshore current to exist. When the sloping shelf and an alongshore density gradient are present, an eastward geostrophically balanced flow can flow onto the shelf, where it is deflected through continuity to flow southwards. In the absence of bottom friction the southward shelf-trapped current increases indefinitely.

5. Conclusions

In this paper we have used both numerical and analytical models to investigate the dynamics of the Leeuwin Current.

In the numerical models, an alongshore density gradient imposed in the Indian Ocean (caused by latitudinal differences in temperature and salinity) produces an eastward flowing geostrophic current that turns poleward on reaching the continental shelf off Western Australia. This current intensifies and deepens as it flows southward, with maximum velocities near the shelf break, and with alongshore current speeds decaying both inshore and offshore. Initially, while the model is spinning up, transient processes dominate the solution. In particular, the eastern boundary current broadens and drifts westward through baroclinic Rossby wave propagation. During the initial stage, however, the alongshore barotropic current on the shelf intensifies, thereby advecting temperature and salinity contours southwards. This advection generates strong fronts, which in turn create thermal winds that enhance the poleward flow seaward of the barotropic current maximum. The numerical results therefore give verification to this speculation of Thompson (1987). Associated with the surface current is an equatorward subsurface countercurrent off the continental shelf. As the deep current flows northward it rises and weakens somewhat in intensity.

The effects of adding warm, fresh North West Shelf waters, possibly arising from Indonesian throughflow, are to enhance the alongshore barotropic flow on the shelf. This effect is mainly confined to the region of the forcing and diminishes with alongshore distance.

An additional experiment having a variable width shelf was also run. The effect was to steer the flow so that both the surface and subsurface currents were trapped nearer to the coast. Off Cape Leeuwin, the narrowing shelf also focussed the surface current to make it more intensified. Another feature which was observed in the numerical simulations was the development of a strong cyclonic circulation off North West Cape.

Amplitudes of the numerical model currents, advection of temperature and salinity contours, and the width, structure and geographical location of the current all agree well with the observations of the Leeuwin Current. This leads us to the conclusion that the Leeuwin Current is driven by an alongshore density gradient in the Indian Ocean with the warm, fresh North West Shelf waters contributing to its intensification in the north.

In view of the steady nature of both the flow and the alongshore density gradient that provides the forcing, a simple analytical model for flow over the continental slope is possible. This model assumes a *frozen* density field and a steady velocity field whereby the steric forcing is balanced by bottom friction over the continental shelf. This shelf region is coupled to a two-layer deep ocean in which the flow is eastward and geostrophic. The model assumes zero inflow from the north at the northward limit of the region. The results of the analytical model agree with the observations and the numerical model for large time on several key points. First, the alongshore current has maximum values near the outer shelf and decays towards the coast under the influence of bottom friction. Second, the alongshore current intensifies with poleward distance; and third, the coastal circulation is fed through an eastward geostrophic flow from the deep ocean. The presence of the sloping continental shelf is necessary for a trapped boundary current to exist. In the absence of a shelf the surface layer adjusts throughout the model ocean, by means of westward baroclinic Rossby wave propagation, to balance the imposed density anomaly with result that there is no net current. When a sloping shelf is present, an eastward geostrophic flow in the open ocean flows onto the continental shelf and is deflected southwards through continuity. The eastward flow continues to flow onto the shelf until it is exactly balanced by an offshore Ekman transport in the bottom half of the top layer, with zero net integrated onshore transport.

Weaver and Middleton (1988) conduct an additional numerical experiment identical to Experiment 1 except the continental shelf is everywhere removed (i.e., the ocean is everywhere 5000 m deep). They show that an initially strong eastern boundary current dissipates westward with net result that there is no southward surface current at the coast. After about 55 days the same feedback mechanism, described above, becomes important. The strong offshore fronts, caused by the initial southward advection, generate thermal winds that feed back to enhance the poleward flow at the surface. Since the alongshore barotropic flow on the shelf in Experiments 1–3 is always present, the net advection is larger and hence the resulting thermal winds are stronger than in the experiment of Weaver and Middleton (1988). Thus the resulting southward flow at the surface is also stronger here in Experiments 1–3.

Unfortunately the analytical model has some limitations, the principal one being that the poleward flow is constrained to the shelf proper, unlike the observations and the numerical model which clearly show the current to be centered near the shelf break. Also, the linear, analytic solutions are unable to model advection of temperature and salinity and so density fronts cannot be generated near the shelf break. As a consequence of this, and the assumed nature of the deep ocean in the analytical model, no predictions can be made as to the nature of any equatorward flowing undercurrent. Overall, the model appears to describe the flow on the shelf quite well, and delineates the simple force balances which obtain.

A second barotropic model, not explicitly considered here, is that of Middleton (1987), in which steady coastal circulation in a uniform density coastal ocean is driven by an imposed alongshore pressure gradient at the boundary of the continental margin. In particular, Middleton (1987) considers forces due to a sinusoidal sea level perturbation on a parabolic shaped continental shelf and slope. Interpreting the imposed sea level gradient as being centered at Dongara and varying sinusoidally with latitude, reference to Middleton (1987, Fig. 5) shows that the coastal flow will draw fluid onto the shelf in the north, with the alongshore velocity increasing to the south and being a maximum at the edge of the continental margin. The model is also qualitatively in agreement with the observations over the shelf, but relies also on a *frozen* density gradient in the Indian Ocean.

One important feature, which has not been directly addressed here, is the observed seasonal reduction of the imposed north–south density gradient and the reduction in the density of the North West Shelf waters, both of which occur in the latter half of the calendar year. In the numerical model we imposed annual mean data, so that in the latter half of the calendar year the north–south density gradient would weaken and the Leeuwin Current would be weaker. In the first half of the calendar year the north–south density gradient would increase yielding a stronger Leeuwin Current. On the North West Shelf similar seasonal phenomena would be observed. A second feature, which has not been considered here, is that of wind forcing (whose effect would be most pronounced in the shallow water on the shelf), and this is liable to modify the strength and location of the Leeuwin Current, especially during the latter half of the calendar year.

In summary, it appears that the Leeuwin Current is predominantly driven by north–south density gradients in the Indian Ocean. The current is further enhanced in the north by warm, fresh North West Shelf waters. The eastward geostrophic flow feeds the current at all latitudes, producing an intensification of the current with distance south, a feature that is enhanced by the narrowing of the shelf toward 33°S. Bottom friction over the continental shelf and the sloping shelf itself appear to play an important role in maintaining the nature of the flow, which rounds Cape Leeuwin and advects warmer waters well into the Great Australian Bight.

Acknowledgments. We are grateful for helpful discussions with J. A. Church, R. S. Gardiner-Garden, J. F. Middleton, A. M. Moore and S. B. Power. The detailed reviews, comments and criticisms of this work by J. S. Godfrey and an anonymous referee are also gratefully acknowledged. We are also thankful to G. C. Cresswell and P. Tildesley for providing us with the satellite photograph shown in Fig. 3 and to Y. Edwards at the UNSW, Mathematical Computing Centre for her computing assistance. This research was funded by Australian Marine Sciences and Technologies Grant 85/994.

REFERENCES

Andrews, J. C., 1977: Eddy structure and the West Australian Current. *Deep-Sea Res.*, **24**, 1133–1148.

Boland, F. M., J. A. Church, A. M. G. Forbes, J. S. Godfrey, A. Huyer, R. L. Smith and N. J. White, 1988: Current meter data from the Leeuwin Current Interdisciplinary Experiment. CSIRO Marine Laboratories Rep. No. 198.

Church, J. A., G. R. Cresswell and J. S. Godfrey, 1988: The Leeuwin Current. *Poleward Flow along Eastern Ocean Boundaries,* S. Neshyba, C. N. K. Mooers and R. L. Smith, Eds. Springer-Verlag Lecture Notes, in press.

Cox, M. D., 1984: A primitive equation, three-dimensional model of the ocean. GFDL Ocean Group Tech. Rep. No. 1.

Cresswell, G. R., and T. J. Golding, 1980: Observations of a south-flowing current in the southeastern Indian Ocean. *Deep-Sea Res.*, **27A**, 449–466.

Csanady, G. T., 1978: The arrested topographic wave. *J. Phys. Oceanogr.*, **8**, 47–62.

——, 1979: The pressure field along the western margin of the North Atlantic. *J. Geophys. Res.*, **84**, 4905–4914.

——, 1985: "Pycnobathic" currents over the upper continental slope. *J. Phys. Oceanogr.*, **15**, 306–315.

Gentilli, J., 1972: Thermal anomalies in the Eastern Indian Ocean. *Nature,* **238**(Physical Sciences), 93–95.

Gill, A. E., 1982: *Atmosphere-Ocean Dynamics.* Academic Press, 662 pp.

Godfrey, J. S., 1984: Notes on the physics of the Leeuwin Current. Unpublished manuscript.

——, and T. J. Golding, 1981: The Sverdrup relation in the Indian Ocean, and the effect of Pacific–Indian Ocean throughflow on Indian Ocean circulation and on the East Australian Current. *J. Phys. Oceanogr.*, **11**, 771–779.

——, and K. R. Ridgway, 1985: The large-scale environment of the poleward-flowing Leeuwin Current, Western Australia: Longshore steric height gradients, wind stresses and geostrophic flow. *J. Phys. Oceanogr.*, **15**, 481–495.

Greig, M. A., J. S. Godfrey, P. Schneider and K. R. Ridgway, 1986: The 'Warreen' sections; temperatures, salinities, densities and steric heights in the Leeuwin Current, Western Australia, 1947–1950. CSIRO Marine Laboratories Report 175, 22 pp.

Hamon, B. V., 1965: Geostrophic currents in the south-eastern Indian Ocean. *Austr. J. Mar. Freshwater Res.*, **16**, 255–272.

Holloway, P. E., and H. C. Nye, 1985: Leeuwin Current and wind distributions on the southern part of the Australian North West Shelf between January 1982 and July 1983. *Austr. J. Mar. Freshwater Res.*, **36**, 123–137.

Killworth, P. D., 1987: Topographic instabilities in level OGCMs. *Ocean Modelling,* **75**, 9–12.

Kundu, P. K., and J. P. McCreary, 1986: On the dynamics of the throughflow from the Pacific into the Indian Ocean. *J. Phys. Oceanogr.*, **16**, 2191–2198.

Legeckis, R., and G. R. Cresswell, 1981: Satellite observations of sea-surface temperature fronts off the coast of western and southern Australia. *Deep-Sea Res.*, **28A**, 297–306.

Levitus, S., 1984: Annual cycle of temperature and heat storage in the world ocean. *J. Phys. Oceanogr.*, **14**, 727–746.

McCreary, J. P., 1981: A linear stratified ocean model of the coastal undercurrent. *Phil. Trans. R. Soc. London,* **A302,** 385–413.

———, S. R. Shetye and P. K. Kundu, 1986: Thermohaline forcing of eastern boundary currents: With application to the circulation off the west coast of Australia. *J. Mar. Res.,* **44,** 71–92.

Middleton, J. H., 1987: Steady coastal circulation due to oceanic alongshore pressure gradients. *J. Phys. Oceanogr.,* **17,** 604–612.

———, and R. E. Thomson, 1985: Steady wind-driven coastal circulation on a β-plane. *J. Phys. Oceanogr.,* **15,** 1809–1817.

Munk, W. H., 1950: On the wind-driven ocean circulation. *J. Meteor.,* **7,** 79–93.

Rochford, D. J., 1962: Hydrology of the Indian Ocean. Part II: The surface waters of the south-east Indian Ocean and Arafura Sea in the spring and summer. *Austr. J. Mar. Freshwater Res.,* **13,** 226–251.

———, 1969a: Seasonal interchange of high and low salinity surface waters off south-west Australia. CSIRO Division of Fisheries and Oceanography Tech. Paper No. 29, 8 pp.

———, 1969b: Seasonal variations in the Indian Ocean along 110°E. Part I: Hydrological structure of the upper 500 m. *Austr. J. Mar. Freshwater Res.,* **20,** 1–50.

Sharma, G. S., 1972: Water characteristics at 200 cl/t in the Intertropical Indian Ocean during the southwest monsoon. *J. Mar. Res.,* **30,** 102–111.

Thompson, R. O. R. Y., 1984: Observations of the Leeuwin Current off Western Australia. *J. Phys. Oceanogr.,* **14,** 623–628.

———, 1987: Continental-shelf-scale model of the Leeuwin Current. *J. Mar. Res.,* **45,** 813–827.

———, and G. R. Cresswell, 1983: The Leeuwin Current and undercurrent. *Trop. Ocean-Atmosphere Newslett.,* **19,** 10–11.

———, and G. Veronis, 1983: Poleward boundary current off Western Australia. *Austr. J. Mar. Freshwater Res.,* **34,** 173–185.

Vennell, R., and P. Malanotte-Rizzoli, 1987: Coastal flows driven by alongshore density gradients. *J. Phys. Oceanogr.,* **17,** 821–827.

Weaver, A. J., and W. W. Hsieh, 1987: The influence of buoyancy flux from estuaries on continental shelf circulation. *J. Phys. Oceanogr.,* **17,** 2127–2140.

———, and J. H. Middleton, 1988: An analytic model for the Leeuwin Current off Western Australia, School of Mathematics, *Appl. Math. Preprint,* No. AM 88/31, University of New South Wales.

Wooster, W. C., and J. L. Reid, 1963: Eastern boundary currents. *The Sea,* Vol. 2, M. H. Hill, Ed. Wiley-Interscience, 253–280.